Nijmegen HEN-330/90

RAPIDITY CORRELATIONS IN π^+p, K^+p AND pp INTERACTIONS at 250 GeV/c

EHS/NA22 Collaboration

Nijmegen
HEN-330/90

RAPIDITY CORRELATIONS IN π^+p, K^+p AND pp INTERACTIONS AT 250 GeV/c

EHS/NA22 Collaboration

V.V. AIVAZYAN[k], I.V. AJINENKO[h], Yu.A. BELOKOPYTOV[h], H. BIAŁKOWSKA[j1], L.V. BRAVINA[e], H. BÖTTCHER[b], F. BOTTERWECK[f], P.V. CHLIAPNIKOV[h], F. CRIJNS[f], A. DE ROECK[a2], E.A. DE WOLF[a3], K. DZIUNIKOWSKA[d1], A.M.F. ENDLER[g], Z.G. GARUTCHAVA[i], N.G. GRIGORYAN[k], P. van HAL[f4], T. HAUPT[f5], D. KISIELEWSKA[d1], W. KITTEL[f], F. MEIJERS[f6], A.B. MICHAŁOWSKA[a], V.I. NIKOLAENKO[h], K. OLKIEWICZ[d1], L.P. PETROVIKH[h], F.K. RIZATDINOVA[e], V.M. RONJIN[h], A.M. RYBIN[h], L. SCHOLTEN[f7], E.K. SHABALINA[e], L.N. SMIRNOVA[e], N.A. SOTNIKOVA[e], O.G. TCHIKILEV[h], L.A. TIKHONOVA[e], A.G. TOMARADZE[i], V.A. UVAROV[h], F. VERBEURE[a], R. WISCHNEWSKI[b].

[a] Universitaire Instelling Antwerpen, B-2610 Wilrijk and Inter-University Institute for High Energies, VUB/ULB, B-1050 Brussels, Belgium
[b] Institut für Hochenergiephysik, D-O-1615 Berlin-Zeuthen, Germany
[c] Department of High Energy Physics, University of Helsinki, SF-00170 Helsinki, Finland
[d] Institute of Physics and Nuclear Techniques of the Academy of Mining and Metallurgy and Institute of Nuclear Physics, PL-30055 Krakow, Poland
[e] Moscow State University, SU-117234 Moscow, USSR
[f] University of Nijmegen and NIKHEF-H, NL-6525 ED Nijmegen, The Netherlands
[g] Centro Brasileiro de Pesquisas Fisicas, 22290 Rio de Janeiro, Brazil
[h] Institute for High Energy Physics, SU-142284 Serpukhov, USSR
[i] Inst. of High Energy Physics of Tbilisi State University, SU-380086 Tbilisi, USSR
[j] University of Warsaw and Institute of Nuclear Problems, PL-00681 Warsaw, Poland
[k] Institute of Physics, SU-375036 Yerevan, USSR

[1] Partially supported by grants from CPBP 01.06 and 01.09.
[2] Now at MPI, Munich, Germany
[3] Bevoegdverklaard Navorser NFWO, Belgium
[4] Now with Ericsson Telecommunicatie B.V., Rijen, The Netherlands
[5] Now at Syracuse Univ., Syracuse, NY, USA
[6] Now at CERN, Geneva, Switzerland
[7] Now with PANDATA, Rijswijk, The Netherlands

Abstract

Two- and three-particle rapidity correlations are analyzed in K^+p and π^+p-interactions at 250 GeV/c. The main contribution to the two- and three-particle correlation functions comes from mixing of events of different multiplicity. The (short range) two-particle correlation remaining after exclusion of mixing is significantly larger for (+−) than for the equal charge combinations, and is positive for a wider range in rapidity difference. FRITIOF and a 2-string DPM are excluded by our data. A quark-gluon (multi-)string model can describe our inclusive correlation function, but needs to be tuned on the short range part. The multiplicity mixing part increases much faster with increasing energy than the short range part. In the central region, our correlation is similar to that observed in e^+e^- and μp collisions at similar energy.

1 Introduction

The study of correlation effects in particle production processes provides information on hadronic production dynamics beyond that obtained from single-particle inclusive spectra. "Forward-backward" multiplicity correlations, rapidity and pseudorapidity correlations, azimuthal asymmetries are major features of particle production processes. The present paper is an analysis of rapidity correlations in K^+p, π^+p and pp-interactions at 250 GeV/c, based on data from the NA22 experiment [1,2] at the CERN SPS with the European Hybrid Spectrometer (EHS).

Correlations in rapidity y have been studied in different experiments on hadron-hadron [3-14], e^+e^- [15] and lepton-nucleon [16] collisions. Strong y-correlations have been observed in all experiments in one form or another, depending on the concrete form of the correlation function, type of interaction, kind of particles, the kinematic region under consideration, etc. However, a clear concept of the origin and the character of the rapidity correlations is still lacking. The main problems encountered in the study of y-correlations are:

1) The pseudo-correlations arising from the addition of events with different particle multiplicity, i.e. with different density in the single-particle rapidity distribution;
2) the effect of energy and momentum conservation;
3) the influence of resonance formation;
4) the influence of Bose-Einstein correlations.

The analysis of these problems will enable us to answer the question whether clusters will have to be introduced as specific physical objects arising in particle production, and what parameters are needed to describe them. An essential question in this connection is the existence of rapidity correlations within groups of three and more particles. Three-particle y-correlations have been studied at the momenta of 32 GeV/c [17] and 200 GeV/c [3] and with ISR at $\sqrt{s}$=31-62 GeV [14]. The existence of these correlations is also studied in the present paper.

Revival of interest in rapidity correlations, furthermore, derives from the fact that the extrapolation to very small rapidity distances is connected to the values of the intermittency parameters [18] recently studied in many experiments [19-23].

The present paper describes an investigation of rapidity correlations giving important information on the origin of the correlation phenomena. The paper includes a comparison of the NA22 data with other experimental results and with Monte Carlo calculations on different quark-parton models: FRITIOF (version 2.0) [24], a two string version of the dual parton model (2-string DPM) [25] and quark-gluon string model (QGSM) [26,27].

The paper is organized as follows. Sect. 2 contains a brief description of the experiment. In Sect. 3 we describe the main features of FRITIOF, DPM and QGSM. Sect. 4 presents the data on the two-particle y-correlations, as well as a comparison with other experiments and with the quark-model predictions. Sect. 5 contains our results for the three-particle rapidity correlations. The main conclusions are given in Sect. 6.

2 The Experiment

The experiment has been performed with the European Hybrid Spectrometer (EHS), using a meson-enriched beam from the SPS accelerator. The present analysis is based on results of the reconstruction of events in the hydrogen filled rapid cycling bubble chamber RCBC, used as a vertex detector, and a downstream spectrometer. A detailed description of the experimental set-up is given in the papers [1,2] and references therein.

Charged particle tracks are reconstructed from hits in the wire-and drift-chambers of the two lever-arm magnetic spectrometer and from measurements in the bubble chamber. The average momentum resolution ($\Delta p/p$) varies from a maximum of 2.5% at 30 GeV/c to around 1.5% above 100 GeV/c.

Events are accepted for the present analysis when measured and reconstructed charge multiplicity are consistent, charge balance is satisfied, no electron is detected among the secondary tracks and the number of reconstructed tracks rejected by our quality criteria is at most 0,1,1,2 and 3 for events with charge multiplicity 2,4,6,8 and >8, respectively. After these cuts, our inelastic sample consists of about 97 000 of π^+p and 34 500 K^+p and 5700 pp events.

Single diffractive events are defined as events of charged particle multiplicity $n \leq 6$ with at least one positive particle having Feynman $|x_F| > 0.88$ and are removed from the sample of non-single-diffractive events. This corresponds to a reduction by 12 500, 4 800 and 840 events, respectively.

For momenta $p_{LAB} < 0.7$ GeV/c, the range in the bubble chamber and/or the change of track curvature is used for proton identification. In addition, a visual ionization scan has been used for $p_{LAB} \leq 1.2$ GeV/c on the full K^+p and pp and 62% of the π^+p sample. Particles identified as protons are removed from the sample. Particles with momenta $p_{LAB} > 1.2$ GeV/c are not identified in the present analysis and are treated as pions.

The loss of events during measurement and reconstruction is corrected for in agreement with the topological cross section data [1].

Corrections for rejected tracks amount to 6-7% of the tracks. They are approximately independent of the multiplicity n and are assumed to be independent of rapidity y. It has been veryfied that the results do not change if the analysis is restricted to a sample of events without track rejections.

3 Quark models

From a comparison of the correlation functions with predictions from recent parton models, it is possible to elucidate the extent to which these correlations are determined by the interaction at the parton level and by the quark fragmentation functions, without involving clusters as specific physical objects.

In the present paper a comparison is performed with three models: FRITIOF [24], a two string version of the dual parton model (2-string DPM) [25] and the quark-gluon string model (QGSM) [27,28].

In FRITIOF each of the colliding particles is excited to form a dipole. The

meson dipole fragments like a quark-antiquark chain in e^+e^--annihilation and the nucleon dipole like a quark-diquark chain in lepton-nucleon collisions. The model includes gluon radiation, hard parton scattering and diffractive-like excitation. The primordial transverse momenta of valence quarks in version FRITIOF 2.0 correspond to a Gaussian distribution with $\langle k_\perp \rangle = 0.42$ GeV/c.

Parameter values are default, except for the width of the Gausian p_x and p_y transverse momentum distribution for primary hadrons (σ_{p_T}=0.44 GeV/c). The models, furthermore, include the production of tensor mesons in the ratio PS:V:T= 50:35:15. When comparing to non-diffractive data, Monte Carlo events satisfying the "diffractive" criteria (see Sect.2 above) are excluded.

In the DPM version used [29], two strings are formed in the interaction. One string is stretched between the meson quark and the proton diquark and the other between the meson antiquark and the single proton quark. The quark fragmentation is performed according to the symmetric LUND model [30]. The parameters $\langle k_T \rangle$, σ_{p_T} and the PS:V:T ratio are the same as in FRITIOF described above. The structure functions of quarks (di-quarks) i and j in hadron $h(ij)$ are of the form

$$f^i(x) = \frac{1}{B(1-\alpha_i, 1-\alpha_j)} x^{-\alpha_i}(1-x)^{-\alpha_j} \qquad (1)$$

where B is the beta-function and $\alpha_{qq} = -1.5$; $\alpha_{\bar{d}} = \alpha_u = 0.5$ and $\alpha_{\bar{s}} = 0$.

The quark-gluon string model [27,28], just as DPM, is based on dual topological unitarization. In addition to the two strings used in our DPM version, in QGSM strings are also formed between sea quarks and anti-quarks of the colliding hadrons.

The distribution functions of valence quarks (diquarks) $f_{V1}(x_1)$ and $f_{V2}(x_n)$ and sea quarks $f_S(x_i)$ in the hadron are of the form:

$$f_{V1}(x_1) = \frac{1}{\sqrt{x_1}}\ ,\ f_S(x_i) = \frac{1}{\sqrt{x_i}}\ ,\ \ldots\ ,\ f_{V2}(x_n) = x_n^\beta\ ,\ \ i = 2, \ldots, n-1 \qquad (2)$$

where β=1.5 for a uu - and 2.5 for a ud-diquark in the proton, $\beta = -0.5$ for the $u, \bar{d}$-quark in π^+ and K^+-mesons and $\beta = 0$ for the $\bar{s}$-quark in the K^+-meson. The transverse momentum distributions of valence and sea quarks in the hadron are of the form $P(k_\perp^2) \sim \exp(-bk_\perp^2)$ with $b = 6.25$ (GeV/c)$^{-2}$ for the cylindrical diagram.

The string breaking algorithm of QGSM is described in [27]. The hadron longitudinal momentum and energy are determined through the variables $z = (E+p_\parallel)_h/(E+p_\parallel)_q$. The quantity z follows the function $f_q^h(z) = (1+\alpha)(1-z)^\alpha$, which at $z \to 1$ coincides with the fragmentation function $D_q^h(z)$ of quark or diquark q into hadron h, obtained in [31]. The power α depends on the flavor of the fragmenting constituent, the kind of hadron and the transverse momentum of the hadron relative to the parton direction [31]. At the string break-up the momenta of the separate quark $\vec{q}_\perp$ and antiquark $-\vec{q}_\perp$ are assumed to be distributed according $P(\vec{q}_\perp) = 3b/[\pi(1+b\vec{q}_\perp^{\,2})^4]$ with $b = 0.34$ (GeV/c)$^{-2}$. The last break of the string is an isotropic two-particle cluster decay. A ratio PS:V=1:1 is used, without addition of tensor mesons.

The model contains different low energy interaction mechanisms with cross sections decreasing with increasing energy according to a power law, as well as diffraction dissociation.

A comparison of our charge multiplicity distributions and our single-particle inclusive spectra has been performed with FRITIOF and 2-string DPM in [1,2] and with QGSM in [28]. In general, all three models reproduce the single-particle inclusive distributions. The multiplicity distributions are best reproduced in QGSM. In particular, this is true at large multiplicity n, where multi-string formation is important.

4 Two-particle rapidity correlations

4.1 Definitions

The two-particle rapidity correlation function is of the form

$$C^{ab}(y_1, y_2) = \rho^{ab}(y_1, y_2) - f\rho^a(y_1)\rho^b(y_2) \tag{3}$$

with

$$\rho^a(y_1) = \frac{1}{\sigma_{inel}}\frac{d\sigma^a}{dy_1} \;\; ; \;\; \rho^{ab}(y_1, y_2) = \frac{1}{\sigma_{inel}}\frac{d\sigma^{ab}}{dy_1 dy_2} \; . \tag{4}$$

Here, y_1 and y_2 are the c.m. rapidities, σ_{inel} the inelastic cross section and a, b represent particle properties, e.g. charge.

The normalization conditions are:

$$\int \rho^a(y_1)dy_1 = \langle n_a \rangle \;\; ; \;\; \iint \rho^{ab}(y_1, y_2)dy_1 dy_2 = \langle n_a(n_b - \delta^{ab}) \rangle \tag{5}$$

$$\iint C^{ab}(y_1, y_2)dy_1 dy_2 = \langle n_a(n_b - \delta^{ab}) \rangle - f\langle n_a \rangle \langle n_b \rangle \tag{6}$$

where $\delta^{ab} = 0$ for the case when a and b are particles of different species and $\delta^{ab} = 1$ for identical particles, and n_a and n_b are the corresponding particle multiplicities.

Most experiments use

$$f = 1 \;\; , \tag{7a}$$

so that the integral over the correlation function (equal to the ratio $\bar{n}^2/k$ of the negative binomial parameters [32]) vanishes for the case of a Poissonian multiplicity distribution. Other experiments use

$$f = \frac{\langle n_a(n_b - \delta^{ab}) \rangle}{\langle n_a \rangle \langle n_b \rangle} \tag{7b}$$

to obtain a vanishing integral also for a non-Poissonian multiplicity distribution. Our values are compared to those for two e^+e^- cases in table 1.

To be able to compare to the various experiments, we use both definitions and denote the correlation function $C^{ab}(y_1, y_2)$ when following definition (7a) and

$C'^{ab}(y_1, y_2)$ when following definition (7b). We, furthermore, use a reduced form of definition (7b),

$$\tilde{C}^{ab}(y_1, y_2) = C'^{ab}(y_1, y_2)/\langle n_a(n_b - \delta^{ab})\rangle. \tag{8}$$

The corresponding normalized correlation functions

$$R^{ab}(y_1, y_2) = \frac{C^{ab}(y_1, y_2)}{f\rho^a(y_1)\rho^b(y_2)} \tag{9}$$

follow the relations

$$\tilde{R} = R' = \frac{1}{f}(R+1) - 1 \ . \tag{10}$$

These are more appropriate than C when comparisons have to be performed at different average multiplicity and are less sensitive to acceptance problems.

The correlation functions defined by expressions (3)-(10), contain the pseudo-correlation due to the summation of events with different charge multiplicity n. We write the correlation function as

$$C(y_1, y_2) = C_{sh}(y_1, y_2) + C_L(y_1, y_2) \ , \tag{11}$$

where the value of $C_L(y_1, y_2)$ is determined by the differences between $\rho_n(y)$ and $\rho(y)$. Then $C_{sh}(y_1, y_2)$ is connected with other correlation mechanisms and determined by the expression

$$C_{sh}(y_1, y_2) = \sum_n P_n C_n(y_1, y_2) = \sum_n P_n \rho_n(y_1, y_2) - \sum_n P_n \rho_n(y_1)\rho_n(y_2) \ . \tag{12}$$

Here

$$P_n = \frac{\sigma_n}{\Sigma_n \sigma_n} \ , \tag{13}$$

and the rapidity densities for each topology are

$$\rho_n(y) = \frac{1}{\sigma_n}\frac{d\sigma}{dy} \quad \text{and} \quad \rho_n(y_1, y_2) = \frac{1}{\sigma_n}\frac{d\sigma}{dy_1 dy_2} \ . \tag{14}$$

The normalized form is

$$R_{sh}(y_1, y_2) = \frac{C_{sh}(y_1, y_2)}{\sum_n P_n \rho_n(y_1)\rho_n(y_2)} = \frac{\sum_n P_n \rho_n(y_1, y_2)}{\sum_n P_n \rho_n(y_1)\rho_n(y_2)} - 1 \ . \tag{15}$$

C'_{sh} and $\tilde{C}_{sh}$ and their normalized forms R'_{sh} and $\tilde{R}_{sh}$ are defined accordingly, with the averages $\langle n\rangle$ and $\langle n_a(n_b - \delta^{ab})\rangle$ replaced by n and $n_a(n_b - \delta^{ab})$, respectively.

4.2 Results

4.2.1 The correlation functions $C(y_1, y_2)$ and $\tilde{C}(y_1, y_2)$.

In Fig.1a,b the correlation functions $C(y_1, y_2)$ and $\tilde{C}(y_1, y_2)$ are given as functions of y_2 for $y_1 = -0.25 \div 0.25$, for the charge combinations $(--)$, $(++)$ and $(+-)$. Both inelastic and non-single-diffractive π^+p, K^+p and pp samples are given. All multiplicities $n \geq 2$ are used. One senses from these figures that:

1. The correlation functions show the well known maximum at $y_1 = y_2 = 0$. The values of $C(0,0)$ and $\tilde{C}(0,0)$ are positive for all charge combinations:
2. $C^{+-}(0,0) > C^{++}(0,0) > C^{--}(0,0)$ and $\tilde{C}^{+-}(0,0) \approx \tilde{C}^{--}(0,0) \approx \tilde{C}^{++}(0,0)$;
3. $\tilde{C}^{++}$ is wider than $\tilde{C}^{--}$;
4. No significant differences are observed for the π^+p and K^+p samples. To increase statistics we, therefore, combine the K^+p and π^+p into one single M^+p sample;
5. The correlation effect in the central region, i.e. the values of $C(0,0)$ and $\tilde{C}(0,0)$, are only slightly reduced when the single-diffractive events are excluded from the analyses.

4.2.2 The y_1-dependence of the correlation functions

The correlation functions $C(y_1, y_2)$ and $\tilde{C}(y_1, y_2)$ for inelastic M^+p interactions at y_1=$\pm$1, $\pm$2, $\pm$3 are presented for the $(--)$ combination in Fig.2a,b, for $(++)$ in Fig.3a,b and $(+-)$ in Fig.4a,b. These correlation functions are non-symmetric with respect to change of sign of y_1. Positive values of $C(y_1, y_2 = y_1)$ and $\tilde{C}(y_1, y_2 = y_1)$ are observed for $(--)$ and $(++)$ at $|y_1| < 1$, while they extend to $|y_1| = 2$ for $(+-)$. For $|y_1| \geq 2$ the structure is very different for the three charge combinations, in agreement with expectations from the effect for the (positive) charge of leading particles and from leading positive or neutral resonances.

4.2.3 The correlation functions $C_{sh}(y_1, y_2)$ and $\tilde{C}_{sh}(y_1, y_2)$.

The correlation functions $C_{sh}(0, y)$ and $\tilde{C}_{sh}(0, y)$ for the different charge combinations are shown in Fig.5, for our non-diffractive M^+p sample. A comparison of Figs.1a and 5a shows that $C_{sh}(0,0) \ll C(0,0)$ for all charge combinations. This means that the main source of correlations in Fig.1a is the summation of events with different multiplicities. One can, however, see from Fig.5 that also other correlation mechanisms (called short range) exist for all charge combinations.

This short range correlation is significantly larger for the $(+-)$ than for the $(--)$ and $(++)$ combinations. Clearly, resonance decays are one source for this difference. For the case of equal charges, Bose-Einstein interference is a possible source. It has been observed in our data [33] and will be further studied in terms of azimuthal correlation in a forthcoming paper. The structure in $\tilde{C}$ for $(++)$ near $y = -3$ is due to the proton cut at $p_{LAB} = 1.2$ GeV/c.

4.2.4 Multiplicity dependence of $C_n(0, y)$ and $\tilde{C}_n(0, y)$

The correlation functions $\tilde{C}_n(0, y)$ are shown in Fig.6 for $(--)$, in Fig.7 for $(++)$ and in Fig.8 for $(+-)$ pairs. Because of the positive charge of both incident particles $n = 2$ does not contribute to negatives, while $n = 4$ contributes to ρ_1 but not to ρ_2. The latter fact leads to the negative contribution for $n = 4$ in Fig.6. For all other n,

$\tilde{C}_n^{--}(0,y_2)$ is positive for $y_2 = y_1 = 0$ and the shape is independent of n.

For $\tilde{C}_n^{++}(0,y_2)$ we see some weak structure at $y_2 = y_1 = 0$, but also in the fragmentation region. With increasing n, however, this effect of leading particles decreases and the shape of $\tilde{C}_n^{++}(0,y_2)$ approaches that of $\tilde{C}_n^{--}(0,y_2)$ at $n \geq 18$.

The correlation $\tilde{C}_n^{+-}(0,y_2)$ in Fig.8 shows the well known maximum at $y_1 = y_2 = 0$. At low n this maximum is approximately Gaussian. With increasing n, it becomes narrower and approaches the shape of $\tilde{C}_n^{--}(0,y_2)$ at $n \geq 18$.

In Fig.9, the values of $\tilde{C}_n(0,0)$ are presented as a function of n and $z = n/\langle n \rangle$. While $\tilde{C}_n^{+-}(0,0)$ is considerably larger than $\tilde{C}_n^{++}(0,0)$ for $n \leq 14$, the three charge combinations may tend to converge at high n.

4.2.5 Comparison with hadron reactions in other experiments

From a comparison of our correlation functions $C(0,y_2)$ and $C_{sh}(0,y_2)$ with the UA5 data [13] (not shown). We deduce that the values of $C(0,0)$ increase strongly with $\sqrt{s}$, while $C_{sh}(0,0)$ increases much weaker (note, that the correlation function for charge-charge (cc) pairs is mainly determined by ($+-$) pairs).

The normalized correlation function $R(0,y)$ for M^+p reactions with $n \geq 8$ is compared to those for pp data from NA23 [4] and ISR [14] in Fig.10. A systematic difference between ISR and EHS is probably due to different experimental biases, but an increase of $R(0,0)$ with $\sqrt{s}$ can be observed separately within the EHS and within the ISR data.

4.2.6 Comparison with e^+e^- and μ^+p-reactions

In Fig.11 we compare the correlation function $\tilde{R}(0,y)$ for our non-single-diffractive M^+p sample ($n \geq 2$) with that for central e^+e^--annihilation at the same energy ($\sqrt{s}$=22 GeV) [15]. The values of $\tilde{R}(0,y)$ are higher for ($++$) pairs than for ($--$) in M^+p reactions, but ($--$) and ($+-$) pairs are in agreement with the correlation in e^+e^- annihilation.

A comparison of the correlation functions for e^+e^--annihilation and non-single-diffractive M^+p collisions throughout the full kinematic region with $y_1 = -1 \div 0$ is shown in Fig.12 for (cc)-pairs. The e^+e^- data are given at $\sqrt{s} = 14$ and 44 GeV [15]. At $y_2 = y_1$ our 22 GeV M^+p correlation lies between the e^+e^- results, but the shape is more symmetric than in e^+e^-.

Fig.13 shows the values of the correlation function $R(y_1,y_2)$ at $y_1 = -0.5 \div 0.5$ for μ^+p-interactions at 280 GeV/c for the energy region of the hadron system $13 < W < 20$ GeV and $n \geq 3$ [34] together with our non-single-diffractive M^+p sample, $n \geq 2$. The μ^+p correlation seems lower than ours, but one has to consider a possible energy dependence. Indeed, extrapolating the energy dependence for $R(0,0)$ published in [34] one would expect a similar value for 22 GeV as found in our experiment.

4.2.7 Model predictions

In the case of e^+e^- [15] and μ^+p collisions [16,34], the LUND Monte Carlo is reported to reproduce the majority of the experimental distributions. In [4] it is shown that this is mainly due to the inclusion of hard and soft gluon effects. However, important underestimates of $R(y_1,y_2)$ are still observable, in particular in the central and current fragmentation regions.

Our results for $C(0,y_2)$ and $\tilde{C}(0,y_2)$ in the combined M^+p non-single-diffractive sample are compared with the FRITIOF 2.0, 2-string DPM and QGSM predictions in Fig.14. As already observed in [4] for $n \geq 8$, FRITIOF and 2-string DPM largely underestimate the correlation. The situation is improved, but not cured, by correcting for the discrepancy in the multiplicity distribution of 2-string DPM [4].

QGSM reproduces $C^{--}(0,y_2)$ very well and even overestimates $C^{++}(0,y_2)$ and $C^{+-}(0,y_2)$. It has been verified that this difference to FRITIOF and DPM is not explained by addition of tensor mesons in the latter.

In Fig.15 we compare FRITIOF and QGSM to the non-single-diffractive data in terms of the short range contribution $\tilde{C}_{sh}(0,y_2)$. The $(+-)$ short range correlation is reproduced reasonably well in both models. For equal charges the strong anti-correlation expected from FRITIOF is not followed by the data. QGSM contains a small equal charge correlation due to a cluster component, but still underestimates its size. These conclusions are supported from a comparison at the various multiplicities n for each charge combination, not reproduced in this paper.

5 Three-particle rapidity correlations

Three-particle rapidity correlations in the central region have been observed at ISR [14] for the normalized inclusive ($n \geq 8$) correlation function in the form:

$$R(y_1,y_2,y_3) = C(y_1,y_2,y_3)/\frac{1}{\sigma^3_{inel}}\frac{d\sigma}{dy_1}\frac{d\sigma}{dy_2}\frac{d\sigma}{dy_3} \tag{16}$$

$$C(y_1,y_2,y_3) = \frac{1}{\sigma_{inel}}\frac{d^3\sigma}{dy_1dy_2dy_3} + 2\frac{1}{\sigma^3_{inel}}\frac{d\sigma}{dy_1}\frac{d\sigma}{dy_2}\frac{d\sigma}{dy_3} - \tag{17}$$

$$-\frac{1}{\sigma^2_{inel}}\frac{d^2\sigma}{dy_1dy_2}\frac{d\sigma}{dy_3} - \frac{1}{\sigma^2_{inel}}\frac{d^2\sigma}{dy_2dy_3}\cdot\frac{d\sigma}{dy_1} - \frac{1}{\sigma^2_{inel}}\frac{d^2\sigma}{dy_1dy_3}\frac{d\sigma}{dy_2}$$

$$\text{with} \qquad \sigma_{inel} = \sum_{n\geq 8}\sigma_n \ .$$

Because of small experimental statistics these correlations failed to be observed in pp-interactions at 200 GeV/c at FNAL [3]. In K^-p interactions at 32 GeV/c [17], three-particle correlations were considered in the form of $\tilde{C}_{sh}(y_1,y_2,y_3)$ and $\tilde{R}_{sh}(y_1,y_2,y_3)$. No positive short-range correlation effect was observed.

The $\tilde{C}_{sh}(y_1,y_2,y_3)$ correlation function is determined as a sum of topological correlation functions:

$$\tilde{C}_{sh}(y_1,y_2,y_3) = \sum_{n\geq 8} P_n\tilde{C}_n(y_1,y_2,y_3) \tag{18}$$

$$\tilde{C}_n(y_1,y_2,y_3) = \tilde{\rho}_n(y_1,y_2,y_3) - \tilde{A}_n(y_1,y_2,y_3) \tag{19}$$

$$\tilde{A}_n(y_1,y_2,y_3) = \tilde{\rho}_n(y_1,y_2)\tilde{\rho}_n(y_3) + \tilde{\rho}_n(y_2,y_3)\tilde{\rho}_n(y_1) + \tilde{\rho}_n(y_1,y_3)\tilde{\rho}_n(y_2) - 2\tilde{\rho}_n(y_1)\tilde{\rho}_n(y_2)\tilde{\rho}_n(y_3)$$

$$\tilde{\rho}_n(y_1, y_2, y_3) = \frac{1}{n(1,2,3)} \frac{1}{\sigma_n} \frac{d^3\sigma}{dy_1 dy_2 dy_3} \tag{20}$$

The functions $\tilde{\rho}_n(y_1, y_2)$ and $\tilde{\rho}_n(y)$ are defined in Sect. 4.1; $n(1,2,3)$ is the mean number of three-particle combinations in events with charge multiplicity n.

The normalized correlation function is defined as:

$$\tilde{R}_{sh}(y_1, y_2, y_3) = \tilde{C}_{sh}(y_1, y_2, y_3) / \sum_n P_n \tilde{\rho}_n(y_1)\tilde{\rho}_n(y_2)\tilde{\rho}_n(y_3) \tag{21}$$

Fig.16 shows the normalized correlation functions $R(0,0,y)$ and $\tilde{R}_{sh}(0,0,y)$ for the combined M^+p sample at 250 GeV/c. Also shown are the values of $R(0,0,y)$ obtained in pp-interactions at $\sqrt{s}$=31-62 GeV [14] (solid lines).

Inclusive three-particle correlations $R(0,0,y)$ are present in our data. They are strongest when a third particle partially compensates the charge of a pair of identical particles. There are, however, no correlation effects in the function $\tilde{R}_{sh}(0,0,y)$. In FRITIOF and QGSM three-particle rapidity correlations are absent in both $R(0,0,y)$ and $\tilde{R}_{sh}(0,0,y)$.

Recently a factorization of the reduced three-particle correlation in terms of a "linked-pair" structure has been proposed [35-37]:

$$R(y_1, y_2, y_3) = R(y_1, y_2)R(y_2, y_3) + R(y_1, y_3)R(y_3, y_2) \tag{22}$$

The comparison of the prediction of (22) to the data is given in table 2, for $n \geq 2$, at a resolution of 0.5 rapidity units. At this resolution, the linked pair ansatz is in agreement with our three-particle correlation within two standard deviations. It is interesting that y correlations are strongly increased when restricting the analysis to low p_T particles, and that the linked pair ansatz also holds there.

6 Conclusions

Two-particle rapidity correlations have been studied in π^+p, K^+p and pp collisions at 250 GeV/c beam momentum.

No big differences are observed in the correlation functions for these three types of reaction. Exclusion of diffractive events does not considerably change the correlation functions.

The main contribution to the correlation function C comes from mixing of events of different multiplicity and different single-particle density, but some effect remains in the so-called short range correlation part. The short range correlation is significantly larger for $(+-)$ than for the equal charge combinations, and is positive for a wider range in $C(y_1, y_2 = y_1)$.

FRITIOF 2.0 and 2-string DPM are excluded by our data on C and $\tilde{C}$. QGSM describes the inclusive correlation function, or even overestimates it.

Because of resonance decay included in the models, all three models give a positive short range correlation effect for unlike pairs, but the effect is not enough to reproduce the data. Probably due the fact that Bose-Einstein interference is

missing in the models, all three fail to reproduce the short range correlation in like charge pairs. Contrary to $C_n(0, y_2)$, the correlation functions $\tilde{C}_n(0, y_2)$ are surpisingly similar for different multiplicity n, except of a narrowing of $\tilde{C}_n^{+-}$ with increasing n. At high multiplicities $\tilde{C}_n$ becomes independent of the charge combination.

$C(0, y_2)$ increases much faster with increasing energy than its short range contribution, and also the reduced correlation function $R(0, y_2)$ shows an increase with increasing energy. In the central region, our correlation is surprisingly similar to that observed in e^+e^- collisions at our energy and to that extrapolated from μp collisions to a hadronic energy of $W = 22$ GeV.

Three-particle correlations are observed in all charge combinations. Within two standard deviations, they are in agreement with the linked pair ansatz. No short range contribution $\tilde{R}_{sh}$ is observed in three-particle correlations. Correlations are particularly large for low p_T particles.

Acknowledgements
It is a pleasure to thank the EHS coordinator L. Montanet and the operating crews and staffs of EHS, SPS and H2 beam, as well as the scanning and processing teams of our laboratories for their invaluable help with this experiment. We are grateful to III. Physikalisches Institut B, RWTH Aachen, Germany, for early contributions to this experiment.

References

1. M. Adamus et al. (NA22): Z. Phys. C - Particles and Fields 32 (1986) 475
2. M. Adamus et al. (NA22): Z. Phys. C - Particles and Fields 39 (1988) 311
3. J. Whitmore: Phys. Rep. 27C (1976) 187
4. J. Bailly et al. (NA23): Z. Phys. C - Particles and Fields 40 (1988) 13
5. V.V. Ammosov et al.: Sov. J. of Nucl. Phys. 23 (1976) 178
6. H. Dibon et al.: Phys. Lett. 44B (1973) 313
7. G. Bellettini et al.: Phys. Lett. 45B (1973) 69
8. L. Foá: Phys. Rep. 22C (1975) 1
9. S.R. Amendolia et al.: Phys. Lett. 48B (1974) 359
10. A. Breakstone et al.: Phys. Lett. 114B (1982) 383
11. V.A. Bumazhnov et al.: Sov. J. of Nucl. Phys. 46 (1987) 289 and 40 (1984) 96
12. I.V. Ajinenko et al.: Serpukhov preprint IHEP 77-45 (1977)
13. R.E. Ansorge et al. (UA5): Z. Phys. C - Particles and Fields 37 (1988) 191
14. A. Breakstone et al.: CERN/EP 88-132; Europhys. Lett.
15. M. Althoff et al.: Z. Phys. C - Particles and Fields 29 (1985) 347
    J. Chwastowski Thesis: Charged Particle Multiplicities and Correlations in e^+e^- Annihilation between 14 and 43.6 GeV, DESY, Hamburg (1988)
16. M. Arneodo et al.: Z. Phys. C - Particles and Fields 31 (1986) 333 and 40 (1988) 347
17. V.A. Bumazhnov et al.: Serpukhov preprint IHEP 79-181 (1979)
18. A. Białas and R. Peschanski: Nucl. Phys. B273 (1986) 703
19. B. Buschbeck, P. Lipa and R. Peschanski: Phys. Lett. B215 (1988) 788
    W. Braunschweig et al. (TASSO): Phys. Lett. B231 (1989) 548
    P. Abreu et al. (DELPHI): Phys. Lett. B247 (1990) 137
20. I. Derado, G. Jancso, N. Schmitz and P. Stopa (EMC): Z. Phys. C. - Particles and Fields 47 (1990) 47
21. I.V. Ajinenko et al. (NA22): Phys. Lett. B222 (1989) 306 and B235 (1990) 373
    C. Albajar et al. (UA1): Nucl. Phys. B345 (199) 1
22. R. Holynski et al. (KLM): Phys. Rev. Lett. 62 (1989) 733; Phys. Rev. C40 (1989) R2449
    M.I. Adamovich et al. (EMU-01): Phys. Rev. Lett. 65 (1990) 412
    K. Sengupta, P.L. Jain, G. Singh and S.N. Kim (EMU-08): Phys. Lett. B236 (1990) 219
23. B. Buschbeck and P. Lipa: Mod. Phys. Lett. A4 (1989) 1871
    W. Kittel and R. Peschanski: Nucl. Phys B (Proc. Suppl.) 16 (1990) 445
    A. Białas: Intermittency '90, CERN-TH-5791/90 (to be publ. in Nucl. Phys. A (Proc. Suppl.))
24. B. Andersson et al.: Nucl. Phys. B281 (1987) 289; Lund preprint LU-TP-87-6 (1987)
25. A. Capella: Europ. Study Conf. on Protons and Soft Hadronic Int. (Erice), R.T. Van de Walle (ed.), (World Scientific, Singapore, 1982) p.199

26. A.B. Kaĭdalov, K.A. Ter-Martirosyan, Sov. J. of Nucl. Phys. 39 (1984) 979 and 40 (1984) 135
27. N.S. Amelin et al.: Sov. J. of Nucl. Phys. 51 (1990) 133 and 51 (1990) 535
28. N.S. Amelin, L.V. Bravina, L.N. Smirnova: Sov. J. Nucl. Phys. 52 (1990) 362
29. E.A. De Wolf: Proc. XV Int. Symp. on Multiparticle Dynamics (Lund), G. Gustafson (ed.), (World Scientific, Singapore, 1984) p.1-29
30. T. Sjöstrand: Comp. Phys. Comm. 27 (1982) 243
31. A.B. Kaĭdalov: Sov. J. of Nucl. Phys. 45 (1987) 902
32. A. Giovannini and L. Van Hove: Z. Phys. C - Particles and Fields 30 (1986) 391
33. M. Adamus et al. (NA22): Z. Phys. C - Particles and Fields 37 (1988) 347
34. P. Malecki: Charged Particle Correlation in Muon-Proton Collisions, Festschrift L. Van Hove, eds. A. Giovannini and W. Kittel (World Scientific 1990) p.159
J. Figiel: Hadronization of Partons in Muon-Nucleon Interactions at 280 GeV/c, Krakow preprint IFJ 1398/Ph (1988)
35. P. Carruthers and I. Sarcevic: Phys. Rev. Lett. 63 (1989) 1562
36. A. Capella, K. Fiałkowski and A. Krzywicki: Phys. Lett. 230B (1989) 149
37. E.A. De Wolf: Acta Phys. Pol. B21 (1990) 611

Table 1

Values for f (see (7b) in the text) for e^+e^- at 14 and 44 GeV [15] compared to our experiment.

	e^+e^-, 14 GeV	e^+e^-, 44 GeV	NA22, M^+p
f^{cc}	1,002	1,035	1,11
f^{+-}	1,032	1,098	1,25
f^{++}	0,894	0,969	0,96
f^{--}	0,894	0,969	1,05

Table 2

Comparison of 3 particle correlation and the prediction from the linked pair ansatz, for non-single diffractive data ($n \geq 2$).

	all p_T		p_T <0.15 GeV/c	
	data	LPA	data	LPA
$R^{---}(0,0,0)$	0.23±0.10	0.30±0.03	2.3±1.7	2.0±0.4
$R^{+++}(0,0,0)$	0.14±0.06	0.21±0.02	1.2±0.6	1.0±0.2
$R^{ccc}(0,0,0)$	0.39±0.04	0.53±0.03	1.9±0.5	1.7±0.2

Figure Captions

Fig. 1 Correlation functions $C(0,y)$ (a) and $\tilde{C}(0,y)$ (b) in π^+p and K^+p-interactions at 250 GeV/c for inelastic (•) and non-single-diffractive events (o). For clarity, open circles are shifted when coinciding with full circles.

Fig. 2 y_1-dependence of $C(y_1,y_2)$ (a) and $\tilde{C}_{sh}(y_1,y_2)$ (b) for $(--)$ pairs.

Fig. 3 Same as in Fig.2, but for $(++)$ pairs.

Fig. 4 Same as in Fig.2, but for $(+-)$ pairs.

Fig. 5 Correlation functions $C_{sh}(0,y)$ (a) and $\tilde{C}_{sh}(0,y)$ (b) in M^+p interactions at 250 GeV/c.

Fig. 6 Topological correlation functions $\tilde{C}_n(0,y)$ in M^+p reactions at 250 GeV/c for $(--)$ pairs.

Fig. 7 Same as in Fig.6. but for $(++)$ pairs.

Fig. 8 Same as in Fig.6, but for $(+-)$ pairs.

Fig. 9 $\tilde{C}(0,0)$ dependence on n and $z=n/\langle n\rangle$ for M^+p interactions at 250 GeV/c. The last $(--)$ point corresponds to $n\geq 16$, the last $(+-)$ and $(++)$ points to $n\geq 18$.

Fig.10 Normalized correlation functions $R(0,y)$ for M^+p reactions at 250 GeV/c, pp interactions at 360 GeV/c and pp-interactions at $\sqrt{s}$=31-62 GeV.

Fig.11 Normalized correlation functions $\tilde{R}(0,y)$ for the M^+p non-single-diffraction sample and e^+e^--annihilation at $\sqrt{s}$=22 GeV [15].

Fig.12 Normalized correlation function $\tilde{R}^{cc}(y_1,y_2)$ at $y_1=-1\div 0$ in the non-single-diffraction M^+p sample at 22 GeV and e^+e^--annihilation at 14 and 44 GeV [15].

Fig.13 Normalized correlation functions $R(0,y)$ for the M^+p non-single-diffraction sample and μ^+p-interactions at 280 GeV/c ($13<W<20$ GeV).

Fig.14 Correlations functions $C(0,y)$ and $\tilde{C}(0,y)$ for M^+p reactions as compared with calculations in FRITIOF ($-\cdot-\cdot-$), DPM (——) and QGSM ($---$) (non-single-diffractive sample).

Fig.15 Correlation functions $C_{sh}(0,y_2)$ for M^+p reactions as compared with FRITIOF ($-\cdot-\cdot-$) and QGSM ($---$).

Fig.16 Three-particle rapidity correlations $R(0,0,y)$ (a) and $\tilde{R}(0,0,y)$ (b) for M^+p interactions at 250 GeV/c. The FRITIOF (dot-dashed) prediction is indicated for the charge combination $(---)$, QGSM (dashed) for $(---)$ and $(--+)$.

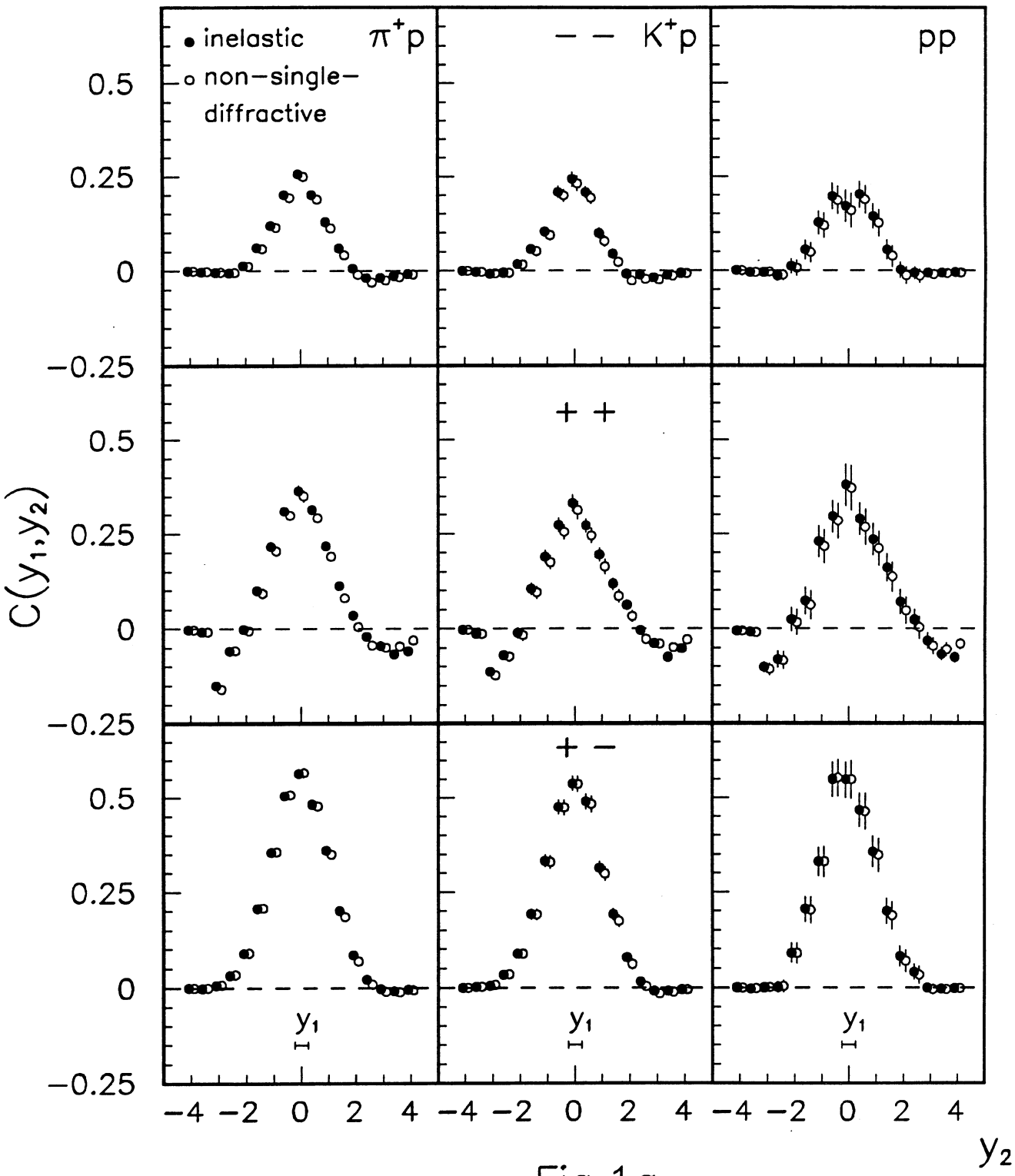
• inelastic
o non−single−
diffractive
π⁺p
− − K⁺p
pp
+ +
+ −
C(y₁,y₂)
0.5
0.25
0
−0.25
−4 −2 0 2 4
y₁
y₂

Fig.1a

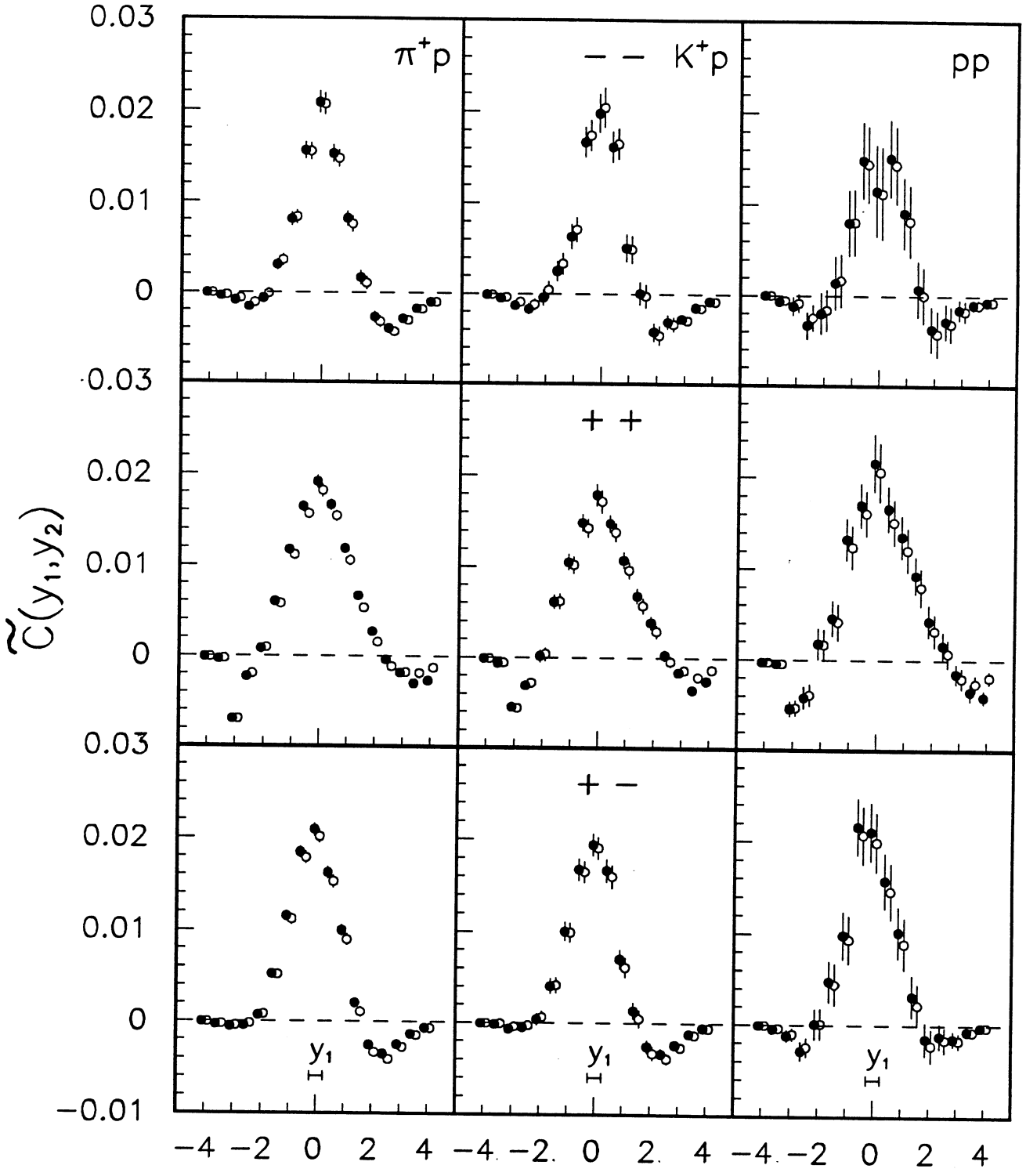
0.03
0.02
0.01
0
-0.03
π^+p
K^+p
pp
++
+-
$\tilde{C}(y_1,y_2)$
y_1
-0.01
-4 -2 0 2 4 -4 -2. 0 2. 4 -4 -2 0 2 4
y_2

Fig.1b

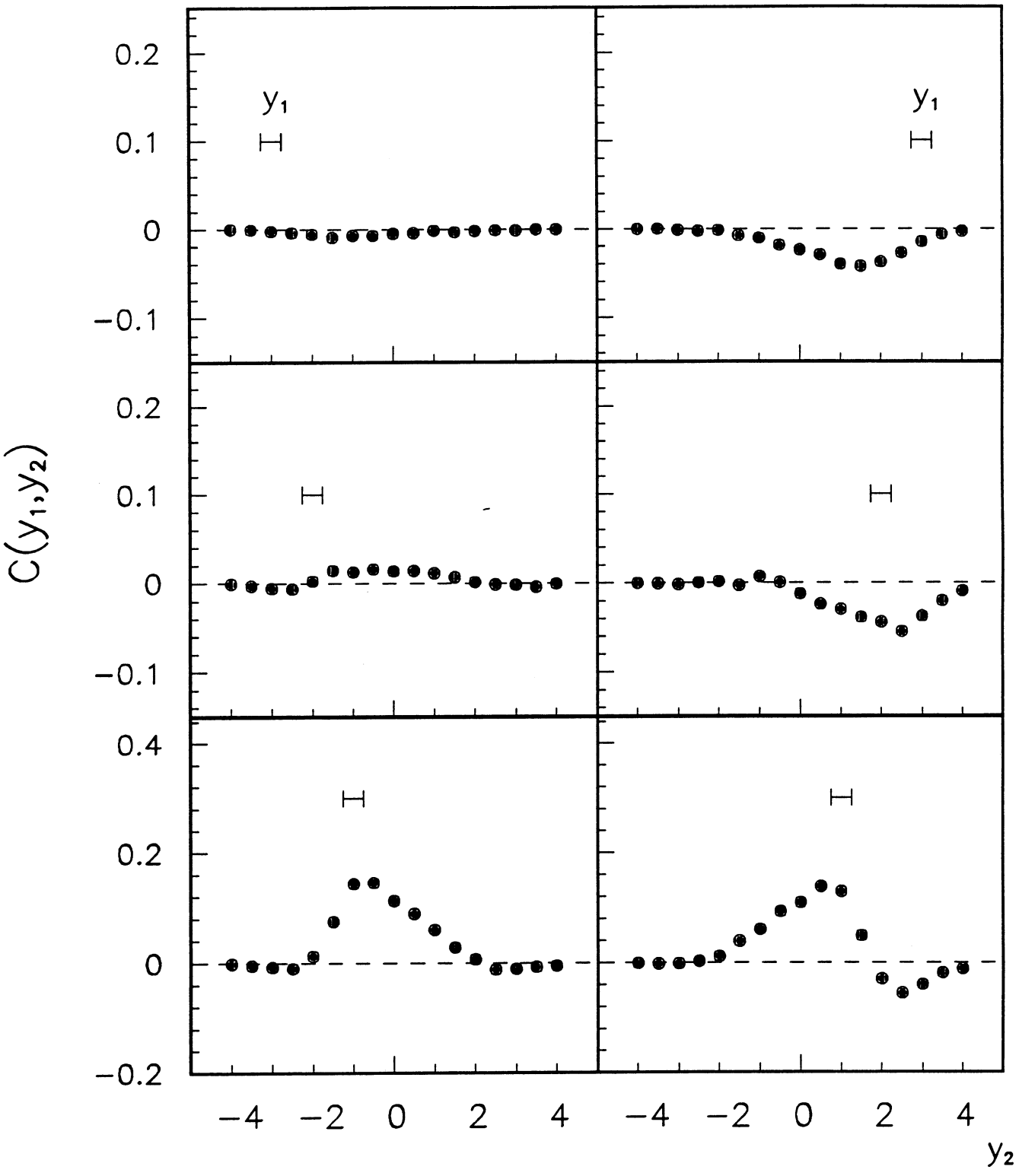

Fig.2a

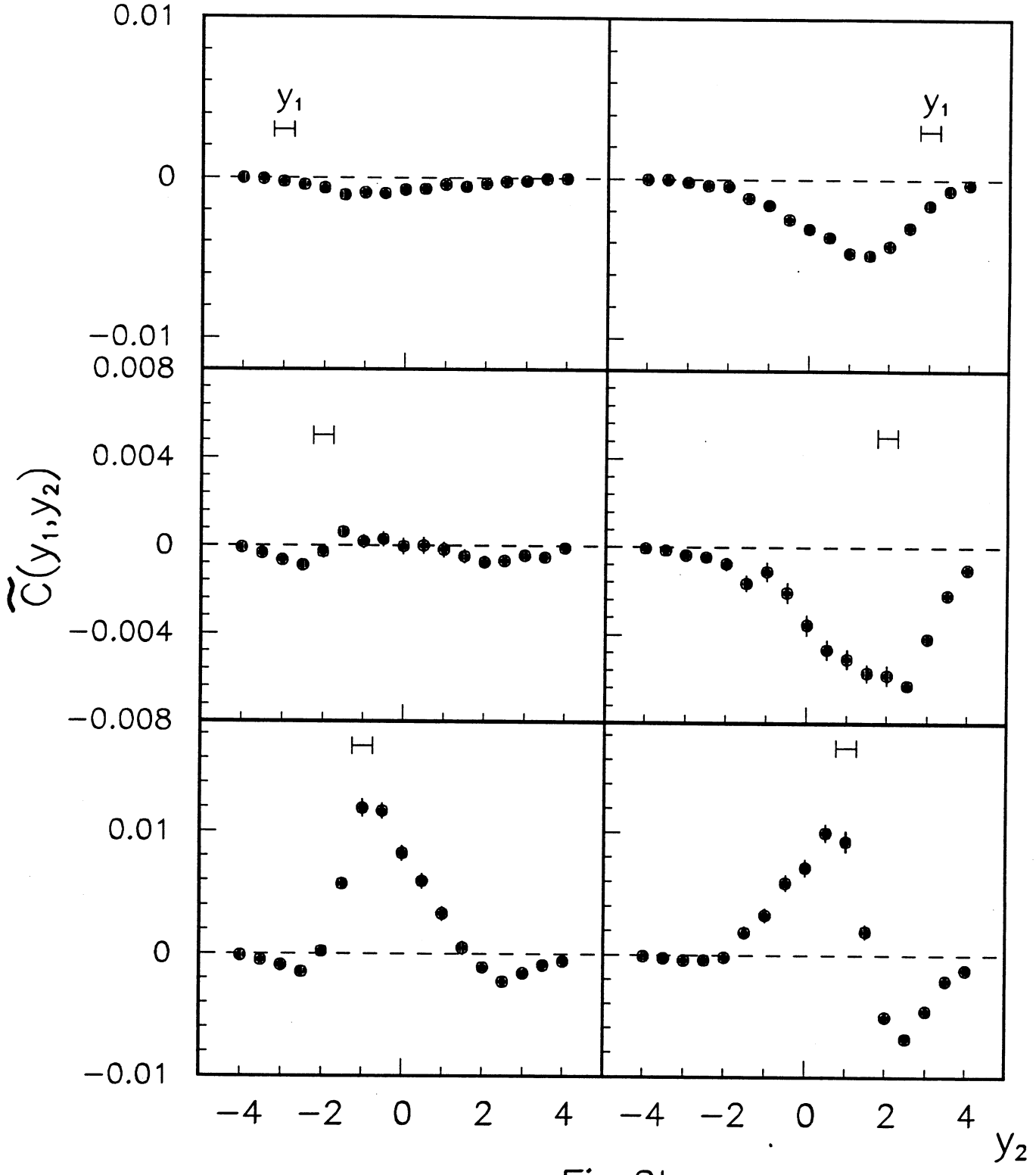
0.01
0
−0.01
0.008
0.004
0
−0.004
−0.008
0.01
0
−0.01
y_1
y_1
$\tilde{C}(y_1,y_2)$
−4
−2
0
2
4
−4
−2
0
2
4
y_2

Fig.2b

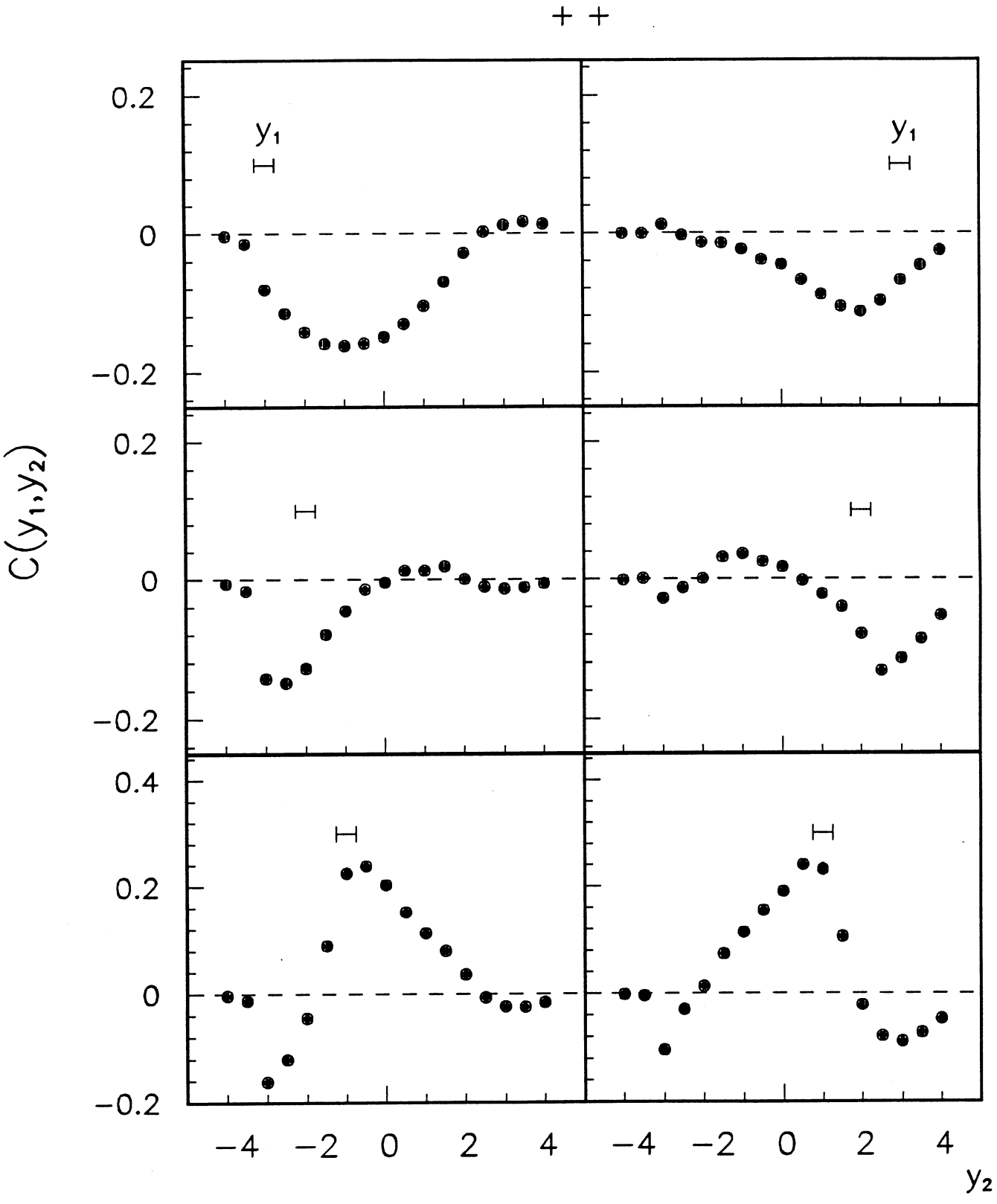

Fig.3a

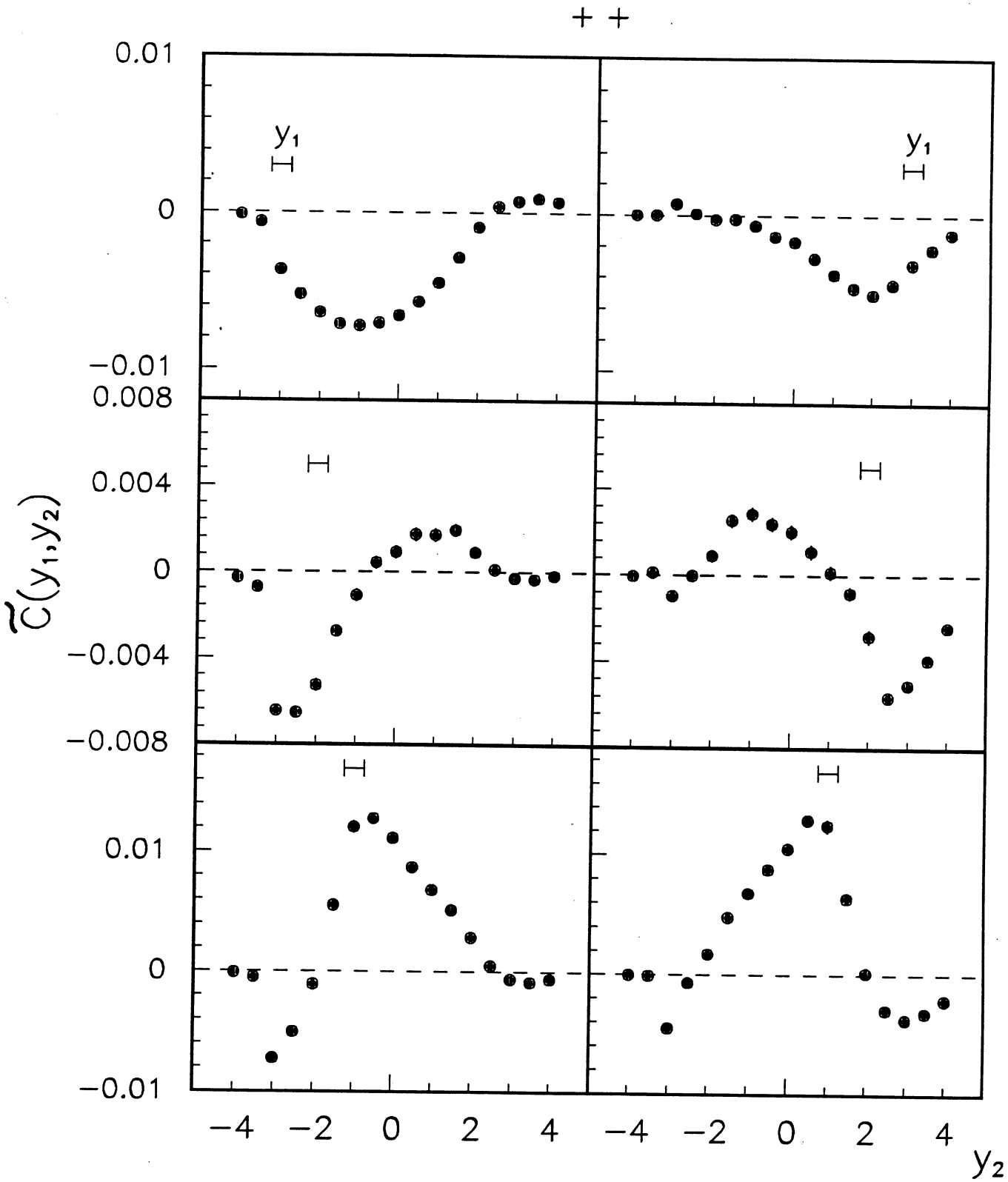
+ +
0.01
0
−0.01
0.008
0.004
0
−0.004
−0.008
0.01
0
−0.01
y_1
y_1
$\tilde{C}(y_1,y_2)$
−4 −2 0 2 4 −4 −2 0 2 4
y_2

Fig.3b

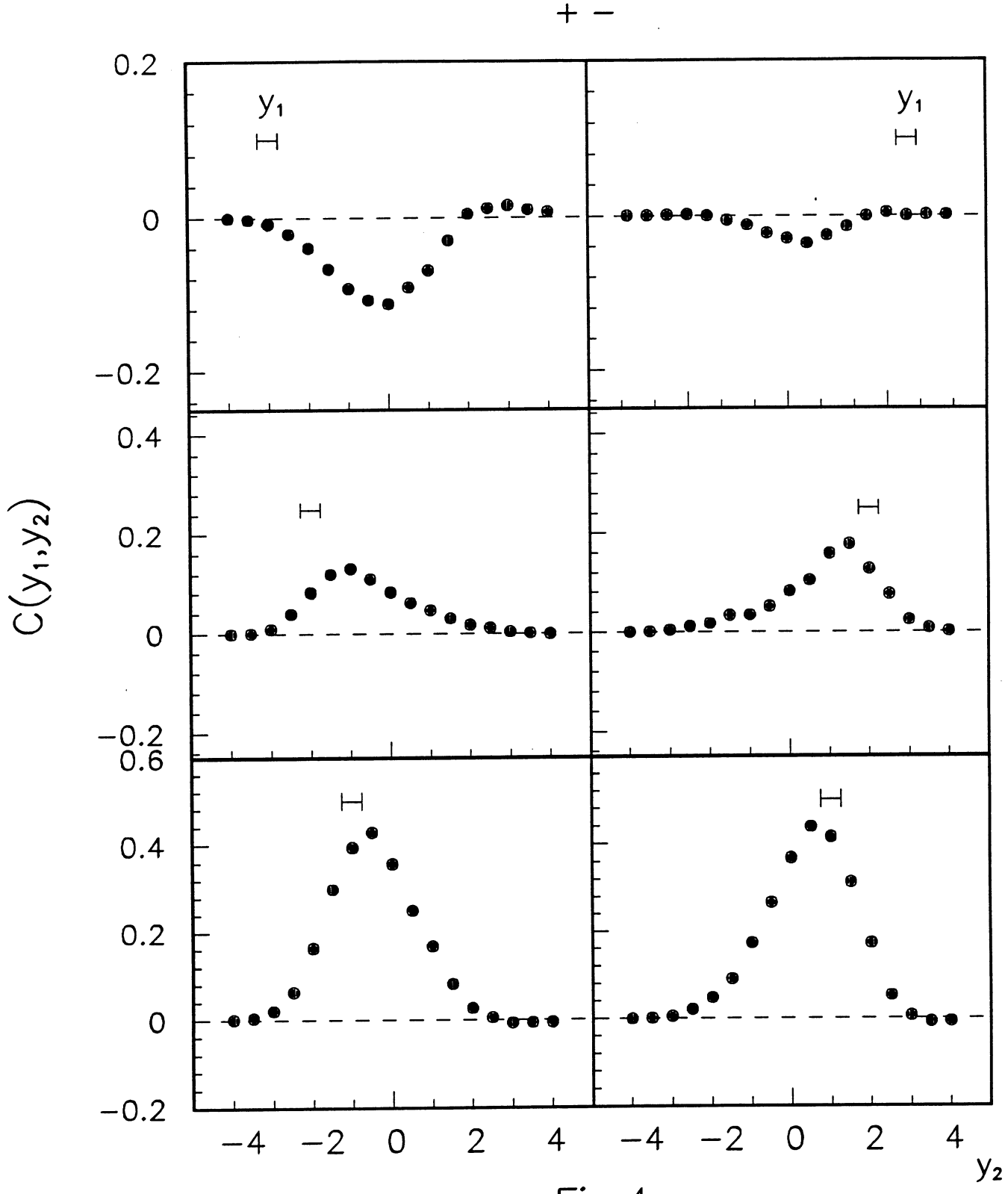

Fig.4a

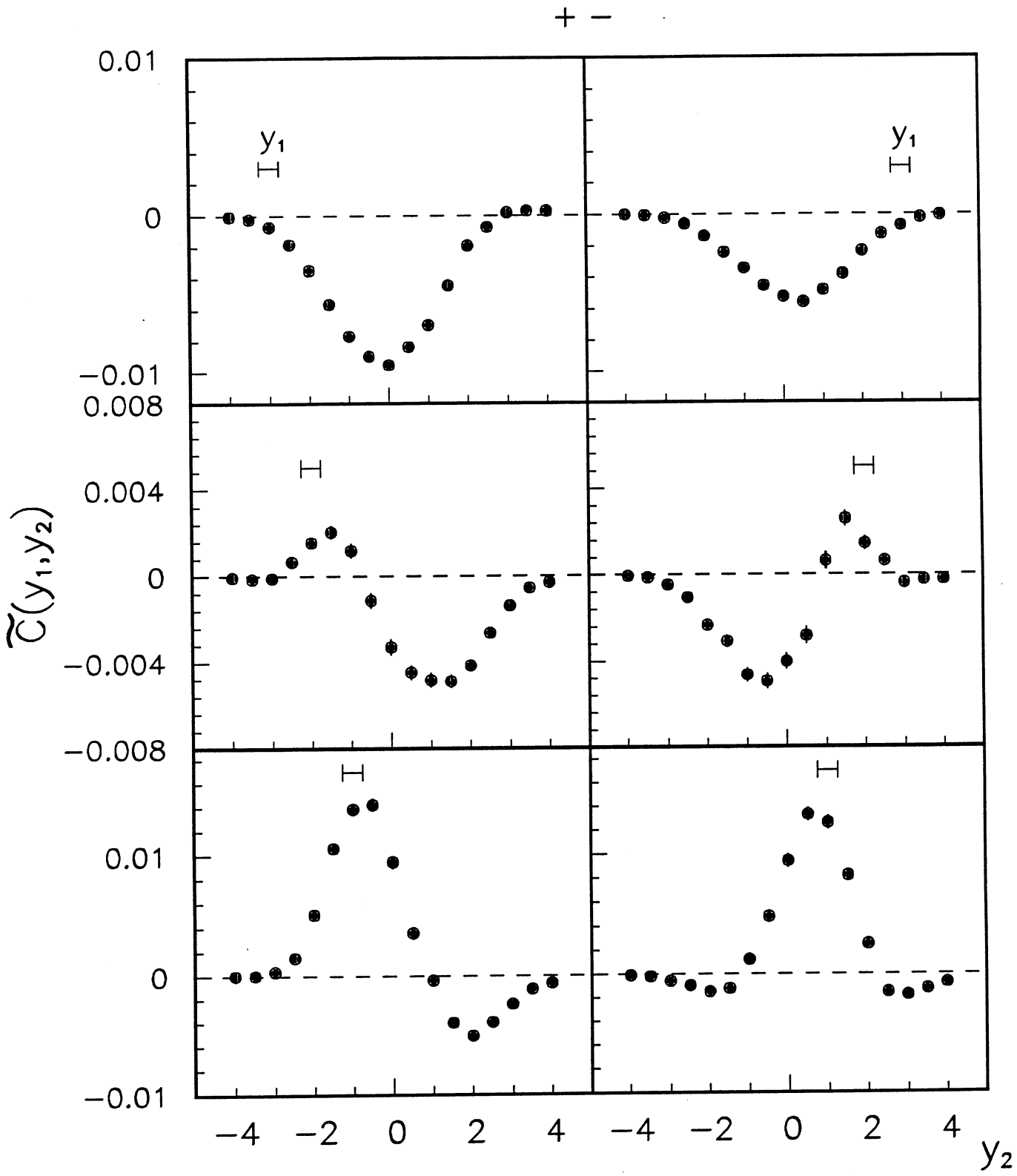
+ −
0.01
0
−0.01
0.008
0.004
0
−0.004
−0.008
0.01
0
−0.01
y_1
y_1
$\widetilde{C}(y_1,y_2)$
−4 −2 0 2 4 −4 −2 0 2 4
y_2

Fig.4b

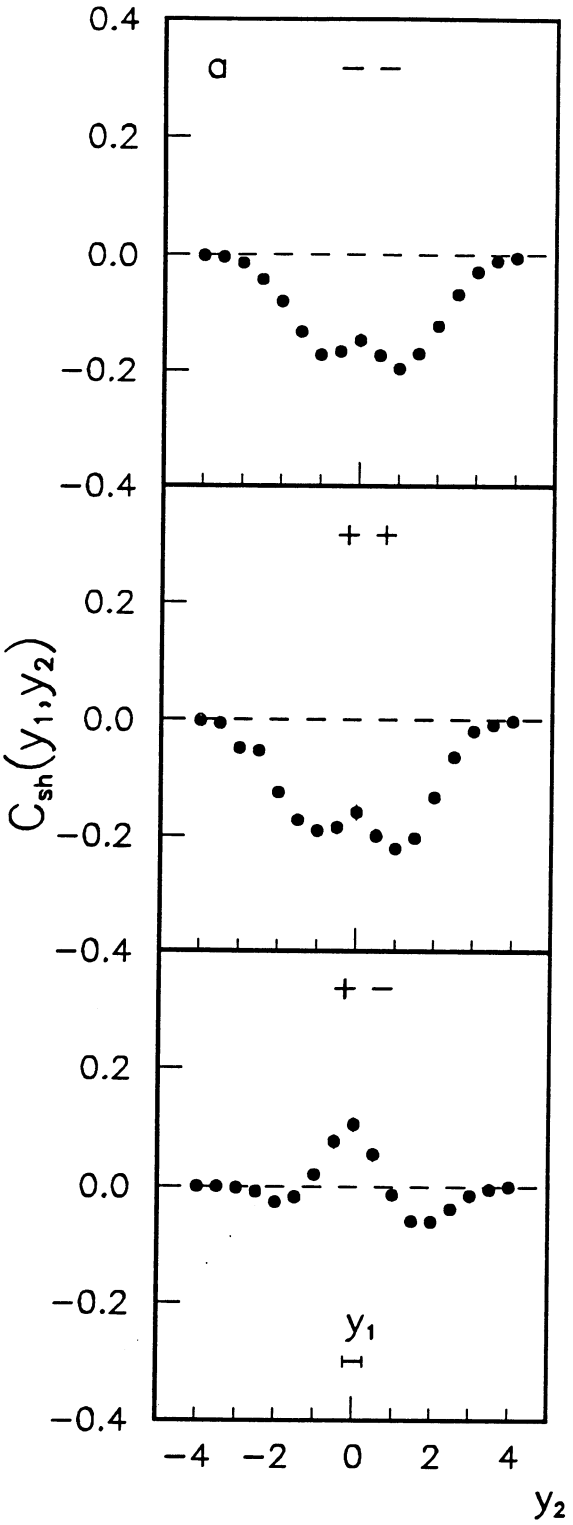
a
− −
+ +
+ −
0.4
0.2
0.0
−0.2
−0.4
$C_{sh}(y_1,y_2)$
y_1
−4 −2 0 2 4
y_2

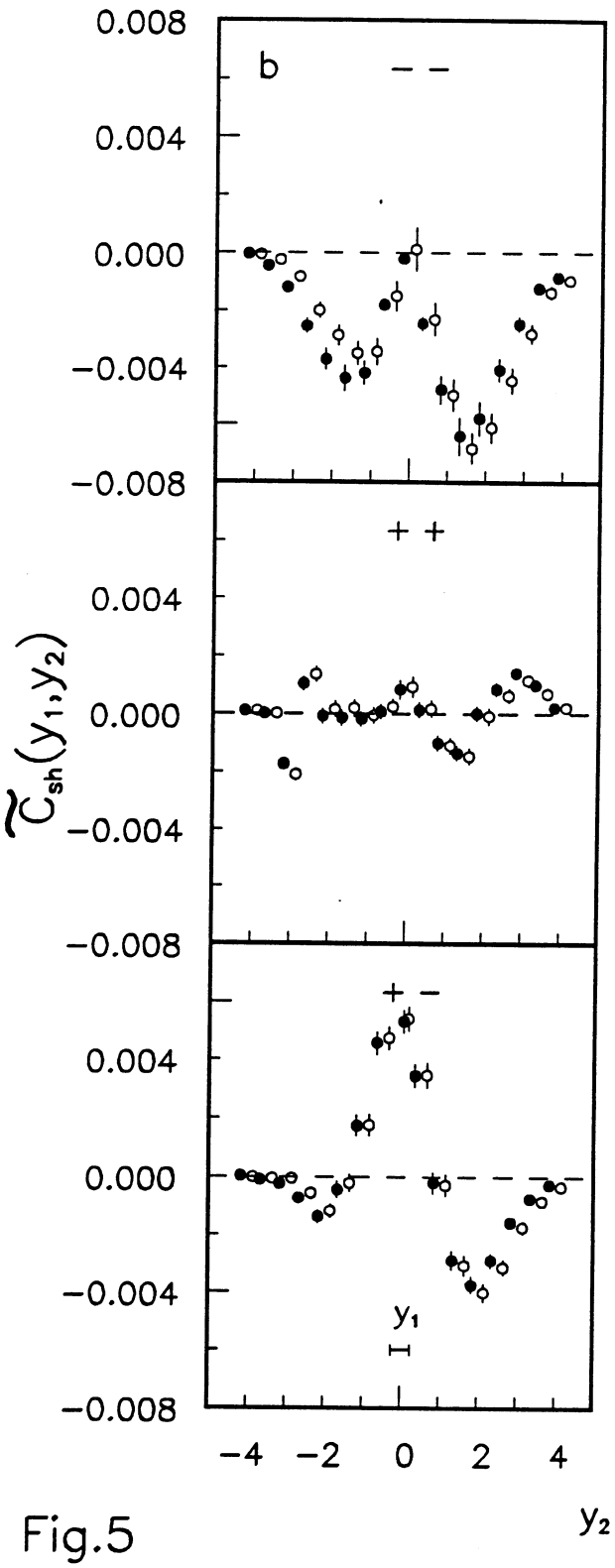
b
− −
+ +
+ −
0.008
0.004
0.000
−0.004
−0.008
$C_{sh}(y_1,y_2)$
y_1
−4 −2 0 2 4
y_2

Fig.5

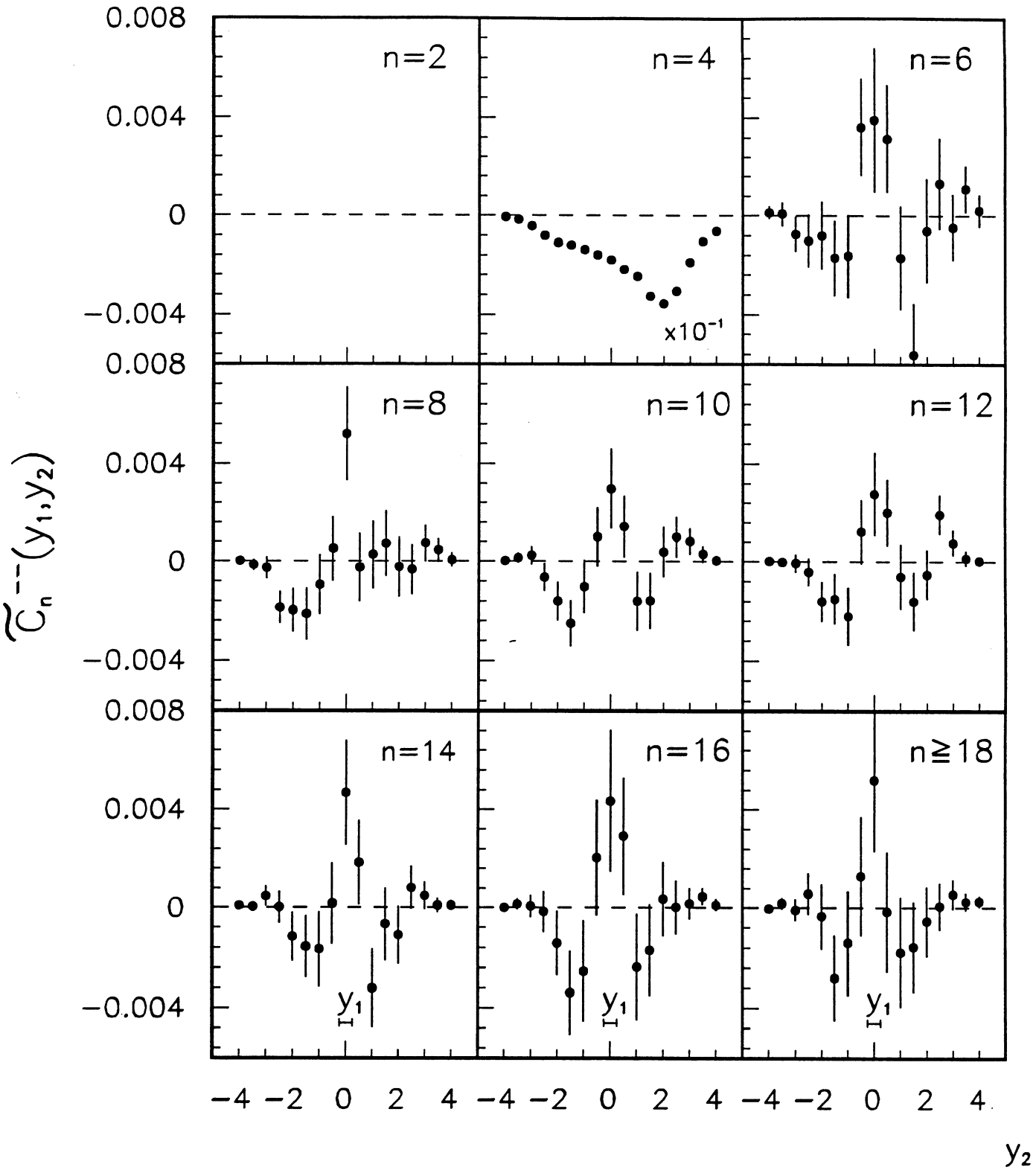
n=2
n=4
n=6
n=8
n=10
n=12
n=14
n=16
n≧18
0.008
0.004
0
−0.004
x10⁻¹
$\tilde{C}_n^{--}(y_1,y_2)$
y_1
y_2
−4 −2 0 2 4

Fig.6

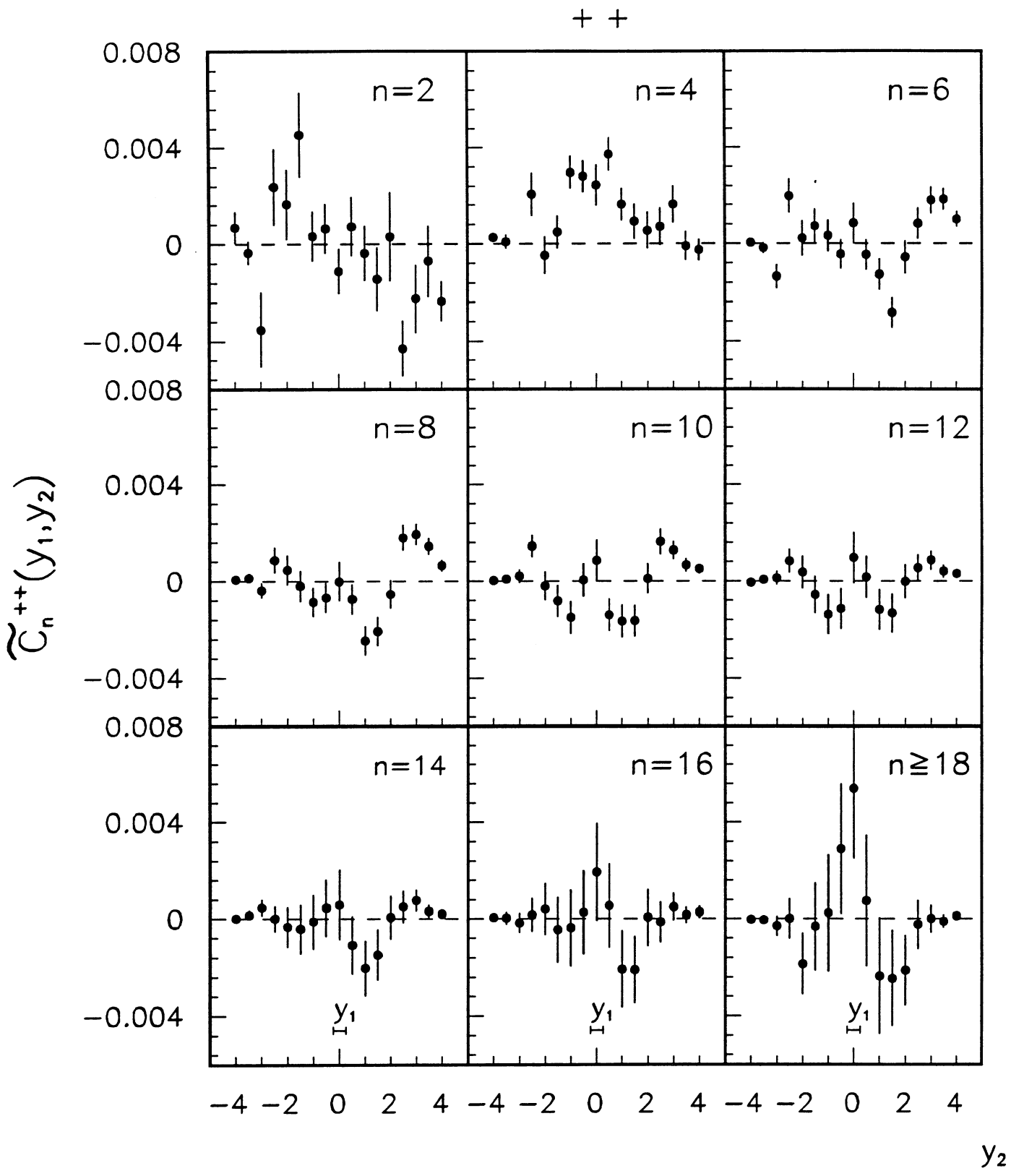
+ +
0.008
0.004
0
−0.004
n=2
n=4
n=6
n=8
n=10
n=12
n=14
n=16
n≧18
$\tilde{C}_n^{++}(y_1,y_2)$
y_1
−4 −2 0 2 4
y_2

Fig.7

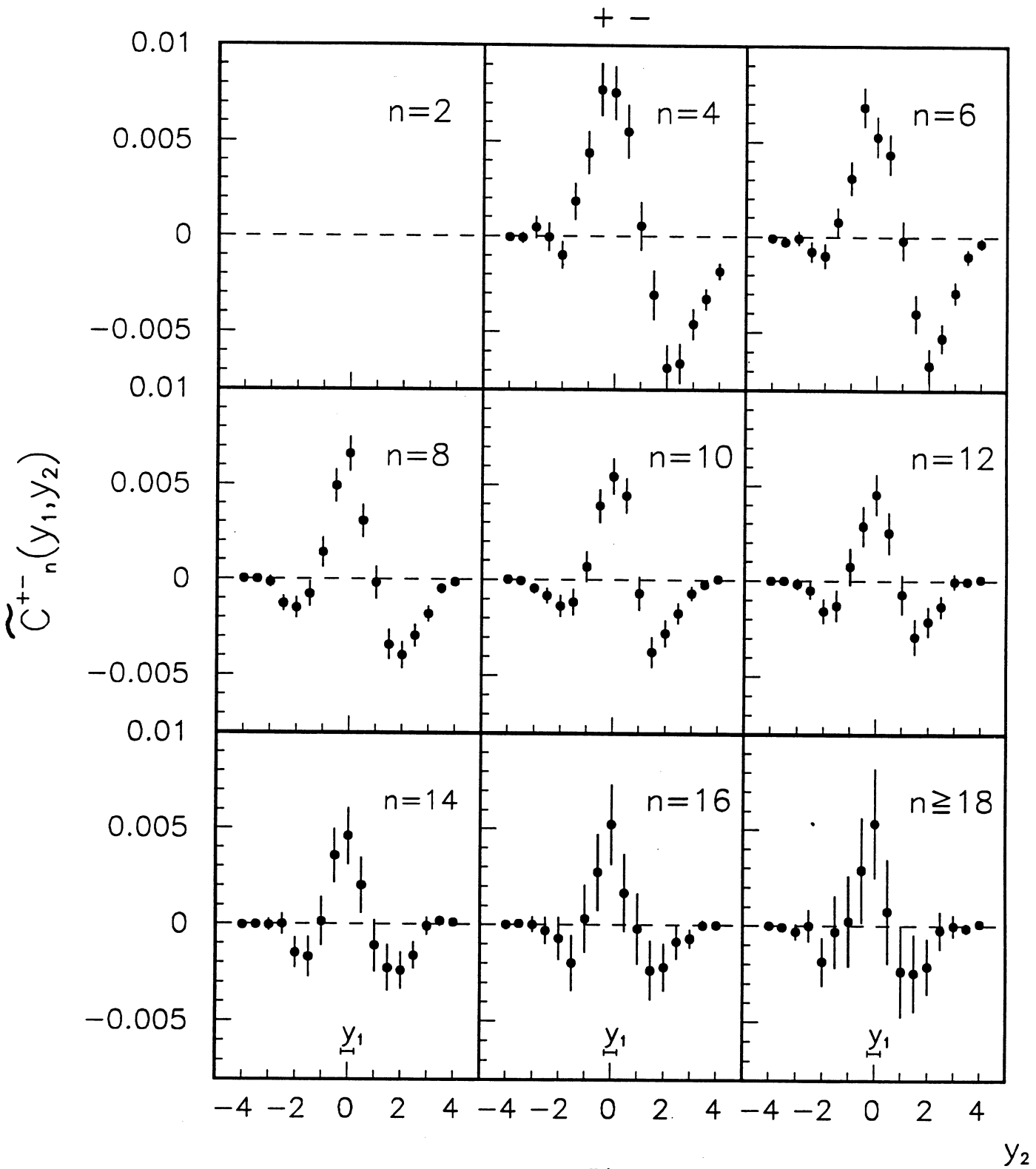
+ −
n=2
n=4
n=6
n=8
n=10
n=12
n=14
n=16
n≧18
0.01
0.005
0
−0.005
−4 −2 0 2 4
y1
y2
$\tilde{C}^{+-}_{n}(y_1,y_2)$

Fig.8

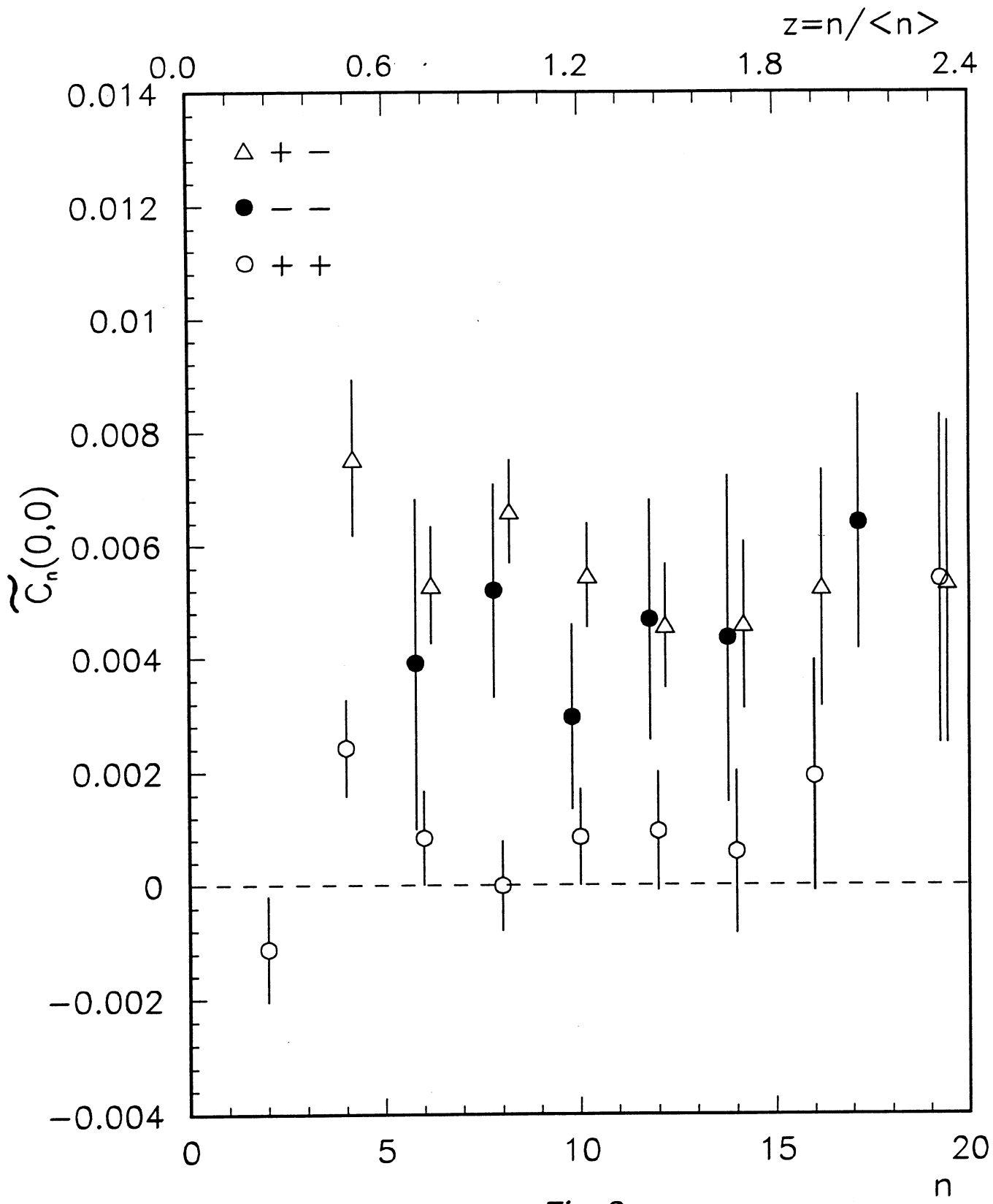
z=n/<n>
0.0
0.6
1.2
1.8
2.4
0.014
0.012
0.01
0.008
0.006
0.004
0.002
0
−0.002
−0.004
△ + −
● − −
○ + +
$\tilde{C}_n(0,0)$
0
5
10
15
20
n

Fig.9

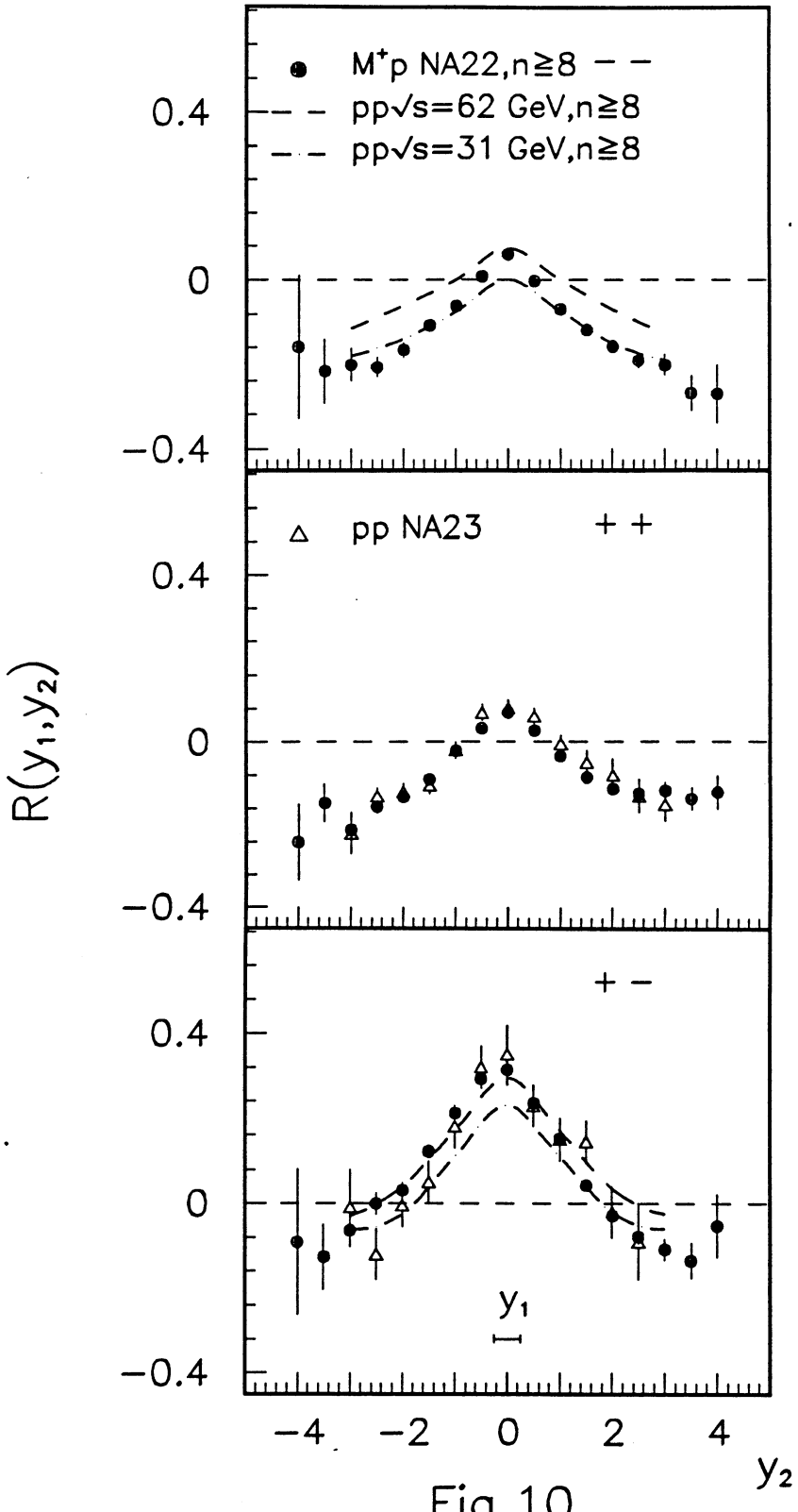
M⁺p NA22,n≧8
pp√s=62 GeV,n≧8
pp√s=31 GeV,n≧8
pp NA23
+ +
+ −
0.4
0
−0.4
R(y1,y2)
y1
−4
−2
0
2
4
y2

Fig.10

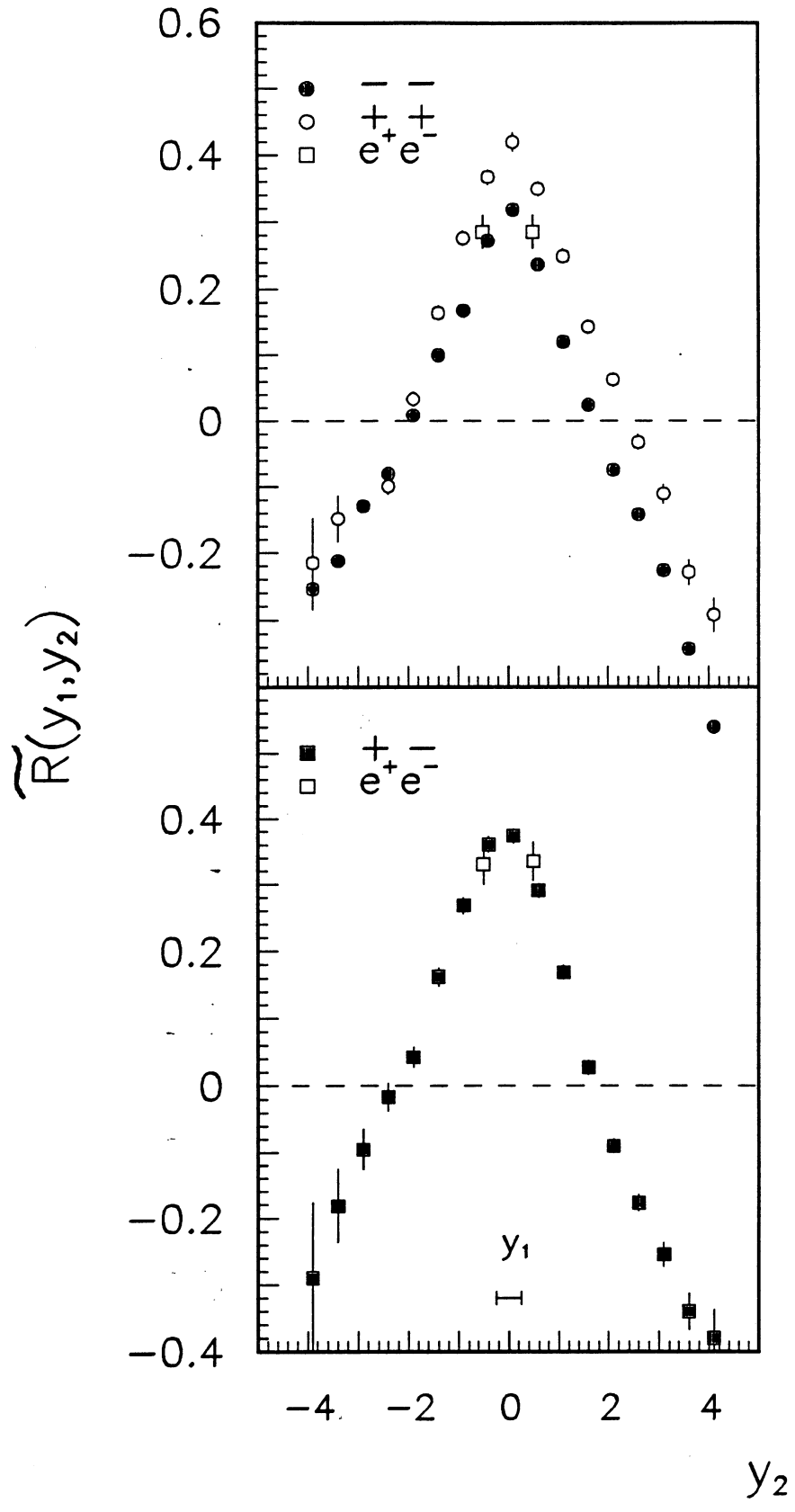

Fig.11

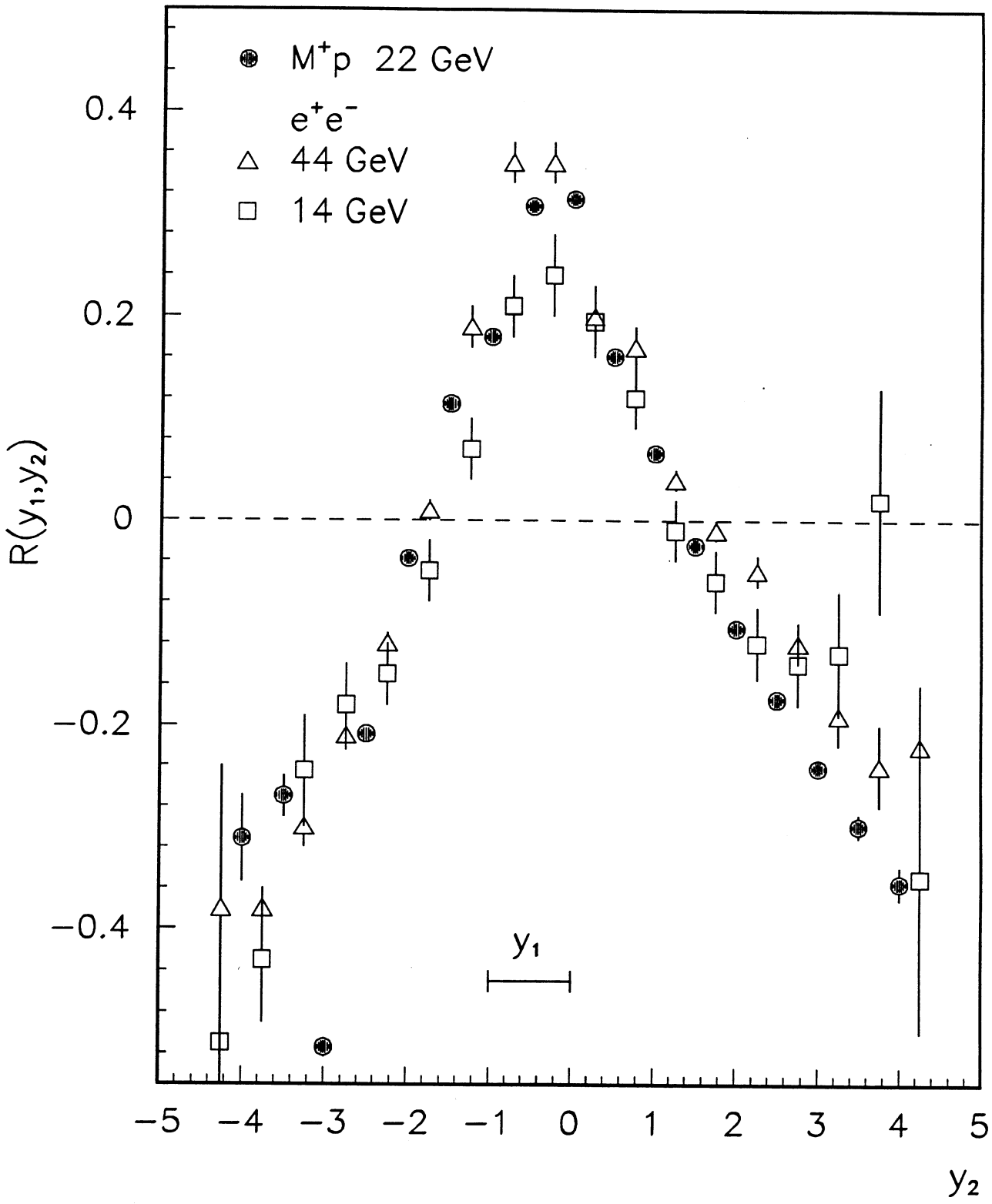

Fig.12

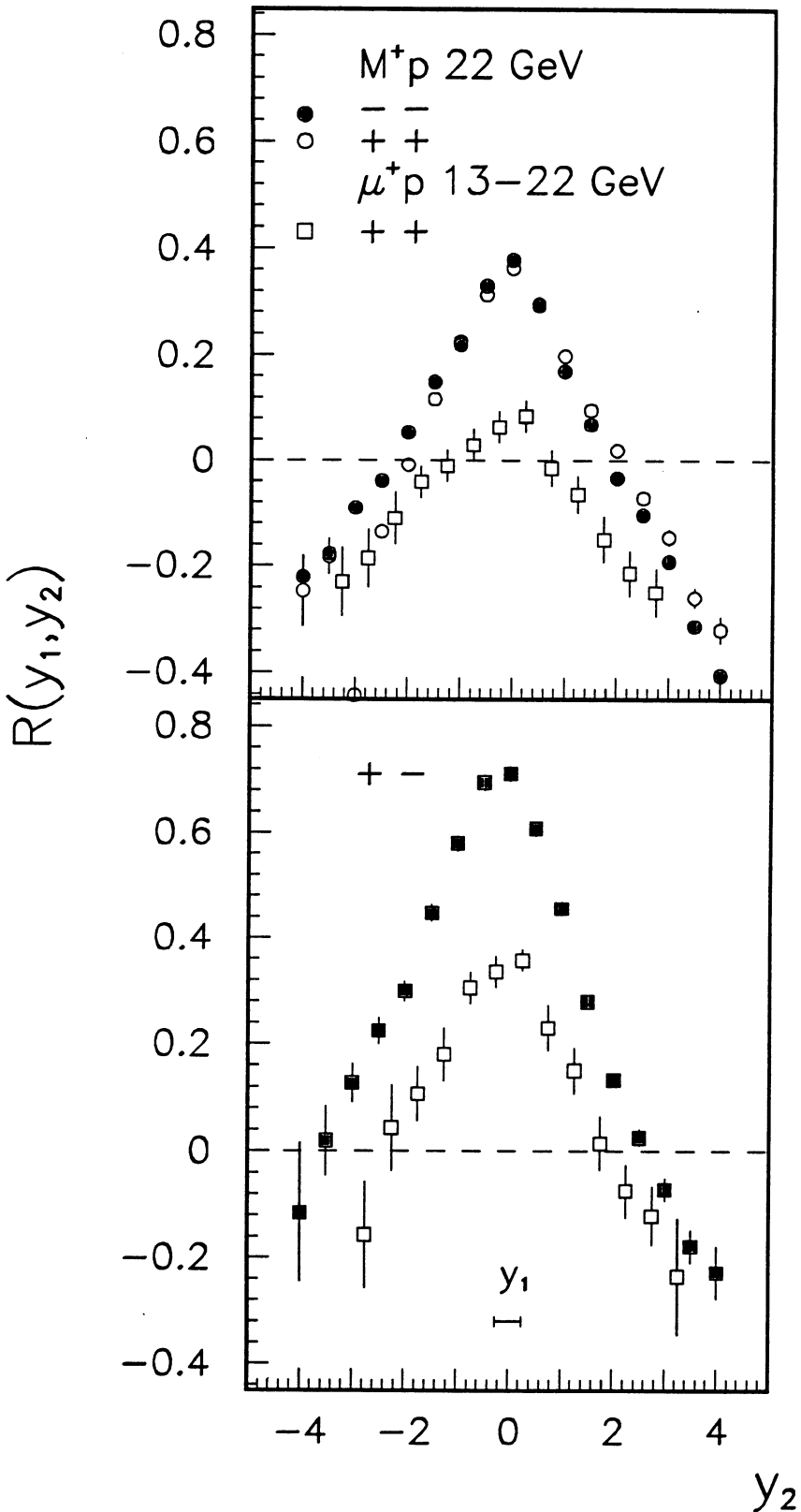

Fig.13

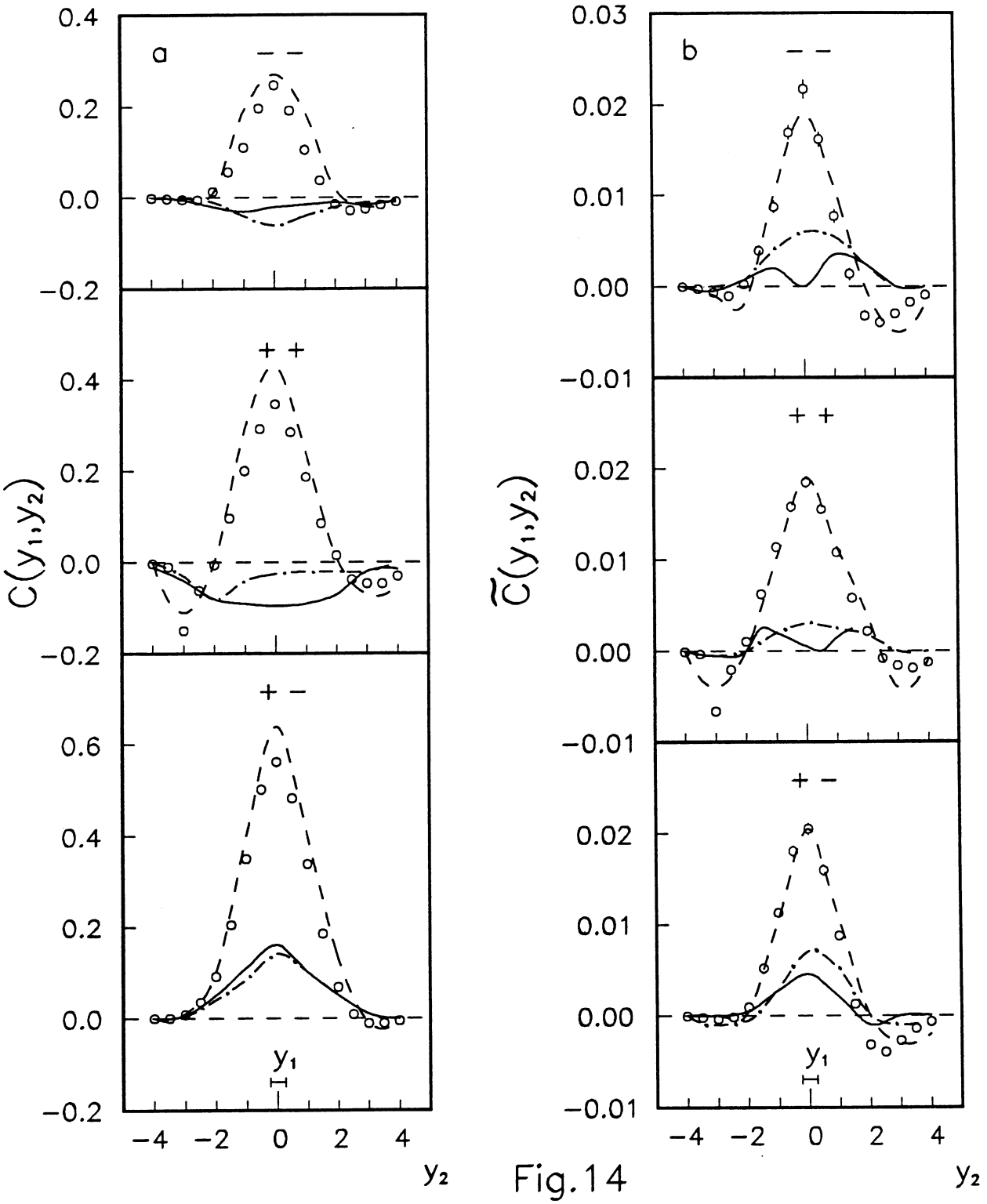

Fig. 14

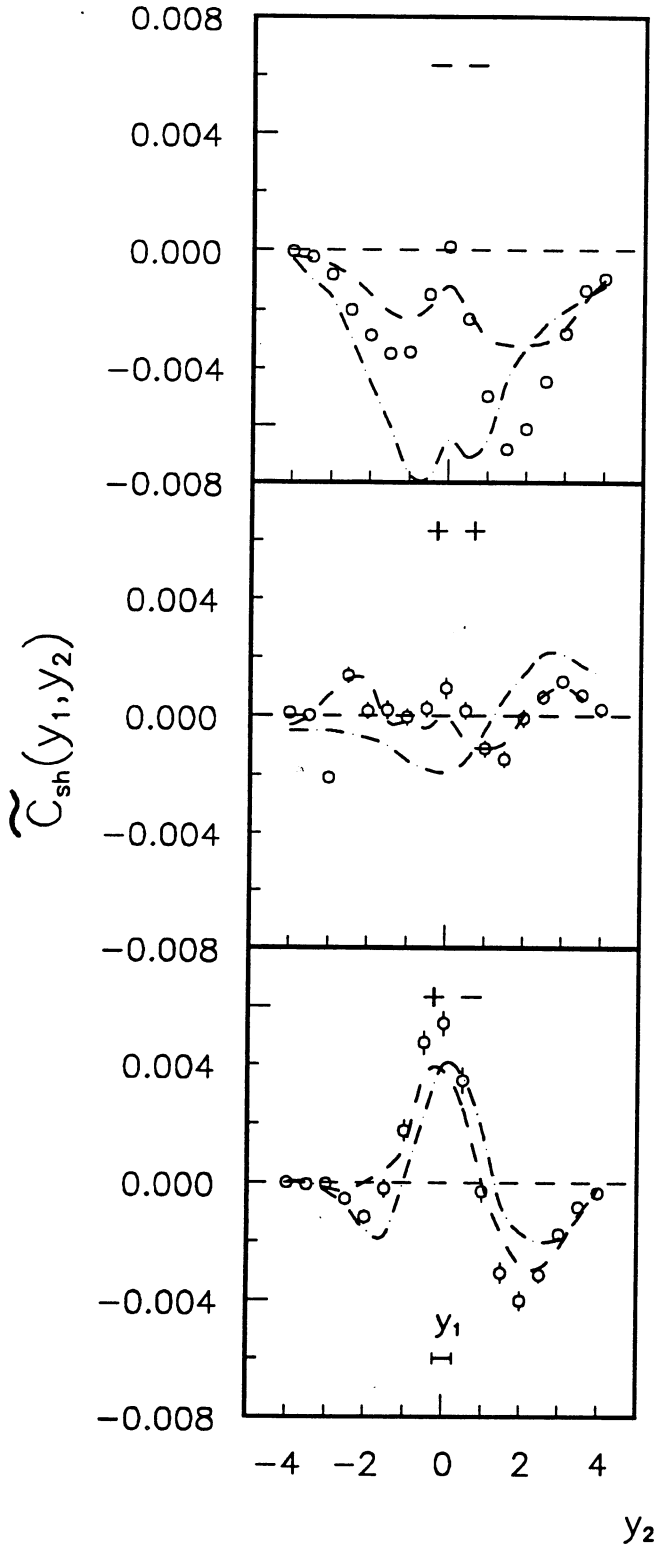

Fig.15

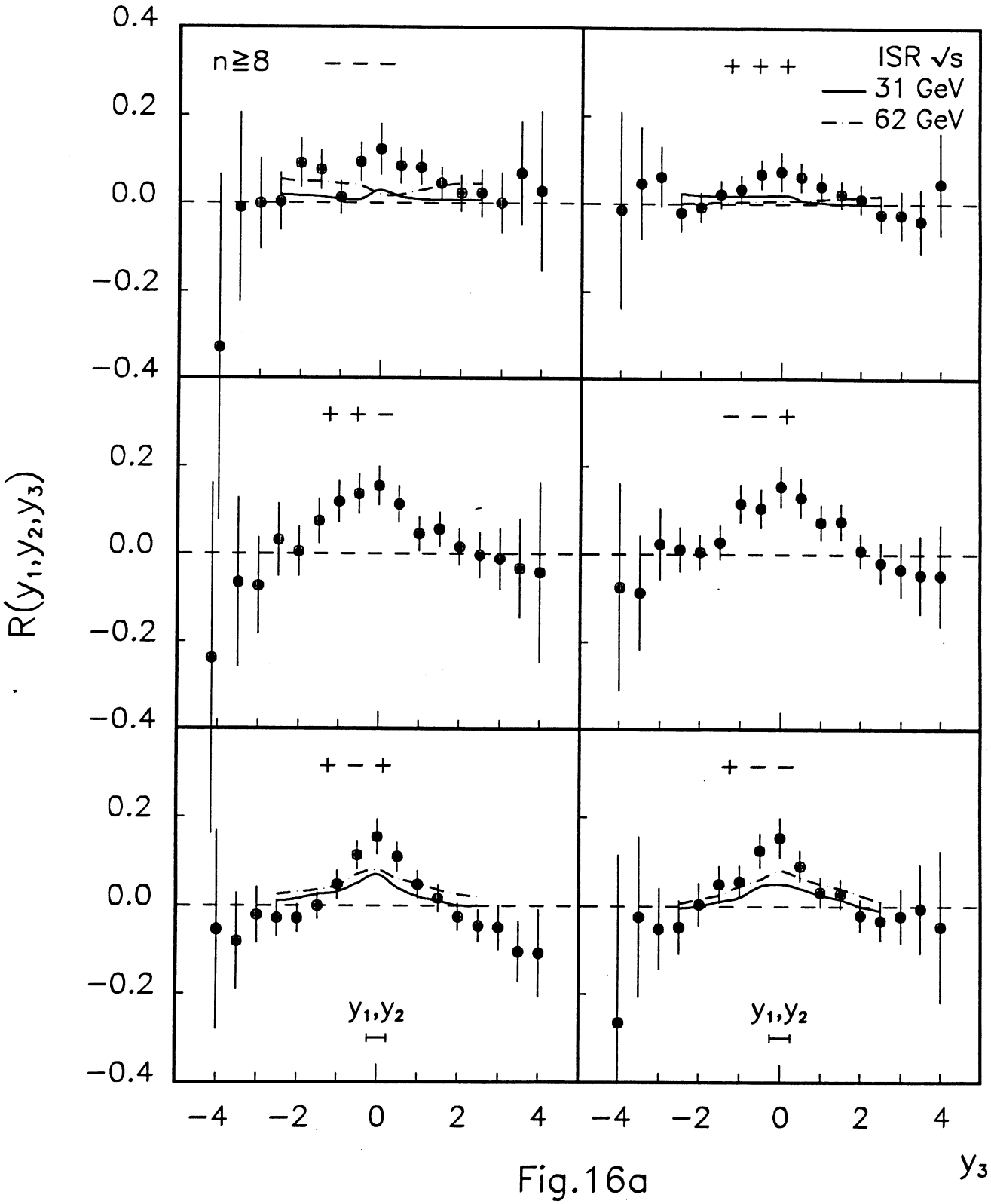

Fig.16a

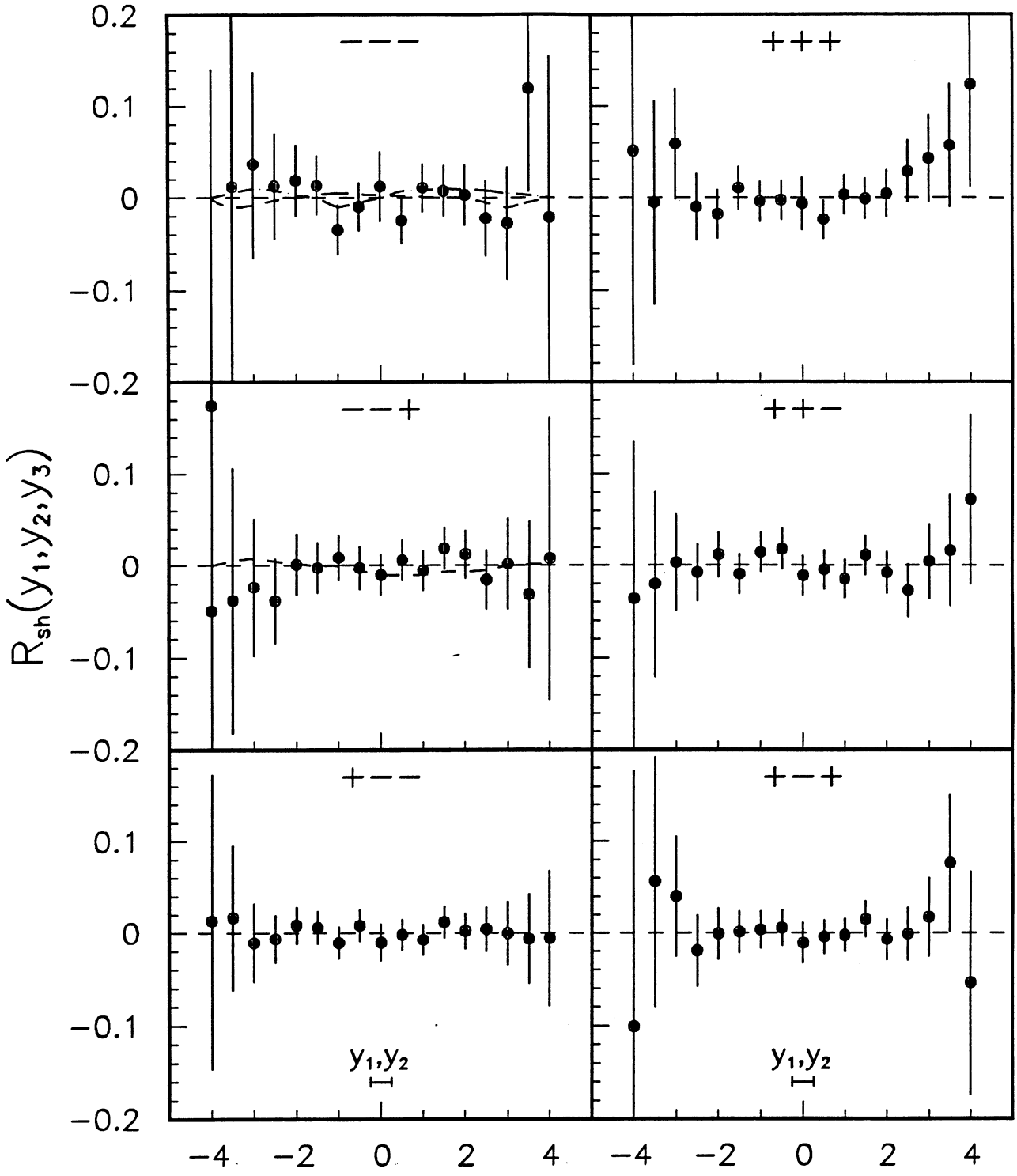

Fig.16b